Ventilation of the North Atlantic Ocean during the Last Glacial Maximum: A comparison between simulated and observed radiocarbon ages

K. J. Meissner, A. Schmittner, and A. J. Weaver
School of Earth and Ocean Sciences, University of Victoria, Victoria, British Columbia, Canada

J. F. Adkins
Geological and Planetary Sciences, California Institute of Technology, Pasadena, California, USA

Received 28 January 2002; revised 27 September 2002; accepted 22 October 2002; published 8 April 2003.

[1] The distribution of radiocarbon during simulations of the Last Glacial Maximum with a coupled ocean-atmosphere-sea ice model is compared with sediment core measurements from the equatorial Atlantic Ceara Rise, Blake Ridge, Caribbean Sea, and South China Sea. During these simulations we introduce a perturbation of North Atlantic freshwater fluxes leading to varying strengths of the Atlantic meridional overturning. The best fit with the observations is obtained for an overturning weakened by 40% compared with today. Further, we simulate the phenomenon of an ''age reversal'' found in deep sea corals, but we suggest that this indicates rather a sudden interruption of deep water formation instead of an increase in ventilation, which was suggested earlier. *INDEX TERMS:* 4860 Oceanography: Biological and Chemical: Radioactivity and radioisotopes; 4255 Oceanography: General: Numerical modeling; 4532 Oceanography: Physical: General circulation; 4267 Oceanography: General: Paleoceanography; *KEYWORDS:* Last Glacial Maximum, thermohaline circulation, radiocarbon, climate modeling

Citation: Meissner, K. J., A. Schmittner, A. J. Weaver, and J. F. Adkins, Ventilation of the North Atlantic Ocean during the Last Glacial Maximum: A comparison between simulated and observed radiocarbon ages, *Paleoceanography*, *18*(2), 1023, doi:10.1029/2002PA000762, 2003.

1. Introduction

[2] From the interpretation of different marine sediment data it is widely believed that the deep water ventilation in the North Atlantic was substantially reduced during the Last Glacial Maximum (21,000 years before present) compared to the present day. The evidence on which this interpretation is based comprises proxy data, such as $\delta^{13}C$ and cadmium, for nutrient distribution, as well as radioactive tracers like radiocarbon (see *Boyle* [1995] for a review).

[3] *Lynch-Stieglitz et al.* [1999] utilize oxygen-isotope ratios of benthic foraminifera, which lived along the ocean margins along the Florida Current during the Last Glacial Maximum (LGM), to infer that the overturning cell was indeed weaker during glacial times. On the other hand, *Yu et al.* [1996] deduce only a relatively small decrease in the oceanic large-scale overturning motion based on $^{231}Pa/^{230}Th$ ratios in sediment cores. *Rutberg et al.* [2000] point out that enhanced biological activity along the North Atlantic continental and ice margins could reduce the signal in the radiochemical data, hiding a glacial-interglacial reorganization of the thermohaline circulation [see also *Boyle and Rosenthal*, 1996]. Moreover, *Marchal et al.* [2000] show that due to the large scatter in the $^{231}Pa/^{230}Th$ data a reduction of the circulation cannot be ruled out.

0883-8305/03/2002PA000762

[4] Previous investigations with coupled ocean-atmosphere-sea ice models [*Meissner and Gerdes*, 2002; *Weaver et al.*, 1998], as well as the ocean modeling studies of *Fichefet et al.* [1994] and *Duplessy et al.* [1996] driven by LGM data [*CLIMAP Project Members*, 1981], all find a weakening of the thermohaline circulation. This view of the glacial circulation, however, has been criticized recently. *Wunsch* [2003] applies an inverse model to the observed radiocarbon distribution and suggests that higher wind stresses during the LGM would have led to higher mass fluxes and that a reduced circulation is thus difficult to rationalize. He also points out that the data base is inadequate to assess mass flux (or ventilation) rates on the grounds of the radiocarbon observations alone.

[5] An alternative method to infer past ventilation rates is through detailed simulations of the glacial circulation including the distribution of those tracers measured in the sediments. The comparison of modeled and observed tracer distributions can then be used to estimate past ocean ventilation rates, which is precisely the objective of the present study. For the LGM, detailed distributions of nutrient tracers have been simulated with a coupled ocean-carbon cycle model [*Winguth et al.*, 1999]. The results from this study indicate that an overturning circulation in the Atlantic with a shallower and 50% weaker flow is most consistent with the observations. Since the nutrient distribution is determined by the marine biology, large uncertainties in its modeling complicate the interpretation of the results. Another recent study also inferred reduced ventilation rates by comparing simu-

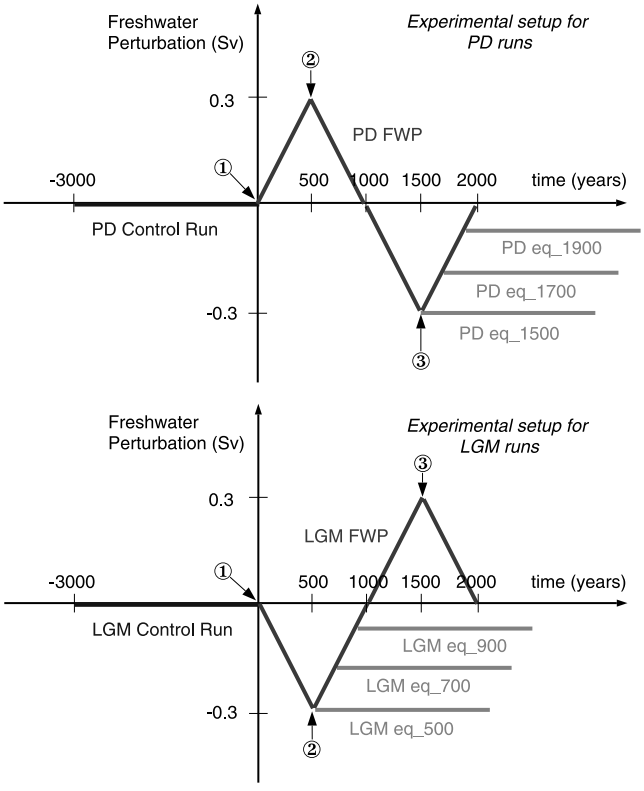

Figure 1. Schematic representation of the experimental design for PD and LGM runs, respectively. The control runs are represented in blue, the freshwater flux perturbation runs in red and the equilibrium runs in green. The points 1, 2 and 3 refer to Figures 2, 3, 7, 8, 9, and 11; 1 represents the end of the control runs and 2 and 3 the maxima and minima of the freshwater forcing. See color version of this figure at back of this issue.

lated sea surface properties with reconstructions [*Schmittner et al.*, 2002a]. However, sea surface properties are only indirectly related to the ventilation.

[6] More direct proxies for ventilation of the deep waters are unstable isotopes like radiocarbon (^{14}C). Since ^{14}C decays with a half-life of 5730 years, waters which have been isolated from the surface for a long time contain considerably lower amounts of ^{14}C than freshly ventilated waters. Measurements of the $^{14}C/^{12}C$ ratio in coexisting benthic and planktonic foraminifera shells from deep sea sediment cores provide a ^{14}C age difference between surface and bottom waters (hereinafter called "top to bottom age difference") [*Broecker et al.*, 1990b]. This top to bottom age difference can give us direct insight in past ocean ventilation rates. Several data sets of top to bottom age differences exist in the North and equatorial Atlantic as well as in the South China Sea for the LGM [*Broecker et al.*, 1990b; *Keigwin and Schlegel*, 2002].

[7] Here we introduce radiocarbon as a radioactive tracer in a coupled ocean-atmosphere-sea ice model. We vary the hydrological budget in the North Atlantic as considerable uncertainties are associated with both its simulation and reconstructions. This leads to different simulated ventilation rates. The modeled top to bottom age differences are then compared to observations in order to find the glacial Atlantic ocean's conveyor circulation in best agreement with deep sea sediment core data. Additionally, we will test the hypothesis whereby age reversals found in deep sea corals from the North Atlantic have been attributed to an abrupt resumption of North Atlantic deep water formation [*Adkins et al.*, 1998].

2. Model Description and Experimental Setup

[8] We use the UVic Earth System Climate Model (ESCM), which consists of an ocean general circulation model (Modular Ocean Model, version 2) [*Pacanowski*, 1995] coupled to a vertically integrated, two-dimensional energy-moisture balance model of the atmosphere and a dynamic-thermodynamic sea ice model [*Bitz et al.*, 2001]. All the subcomponents of the model have the same resolution of $1.8° \times 3.6°$. The vertical resolution of the ocean model varies from 50 m at the surface to 500 m at 5 km depth. The model version used here is described by *Weaver et al.* [2001]. It is driven by seasonal variations in solar insolation at the top of the atmosphere and seasonally varying wind stress at the ocean surface [*Kalnay et al.*, 1996]. Boundary conditions for the Last Glacial Maximum (LGM) simulations are the same as in the work of *Weaver et al.* [1998]. We use elevated topography based on a reconstruction of Northern Hemisphere ice sheets [*Peltier*, 1994]. The planetary albedo is raised by 0.18 over continental ice sheets, the orbital parameters are set to 21 kyr BP values and the level of atmospheric CO_2 is lowered to 220 ppm. All experiments presented here are computed with near surface advection of

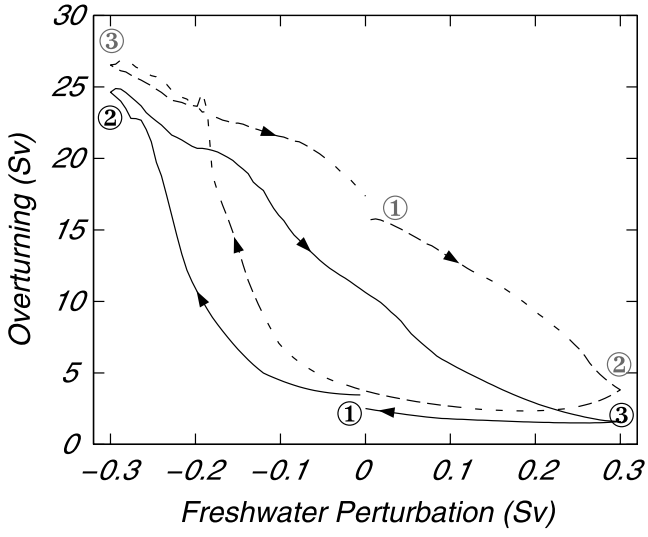

Figure 2. Hysteresis behavior of the Atlantic overturning motion under present-day (dashed) and glacial conditions (solid), respectively. The maximum of the overturning motion is shown as a function of a linearly decreasing (upward branch) or increasing (downward branch) freshwater perturbation in between 50°N and 70°N, changing at a rate of 0.6 Sv/1000 years. The points 1, 2 and 3 indicate the end of the control runs and the maxima and minima of freshwater forcing (see Figure 1).

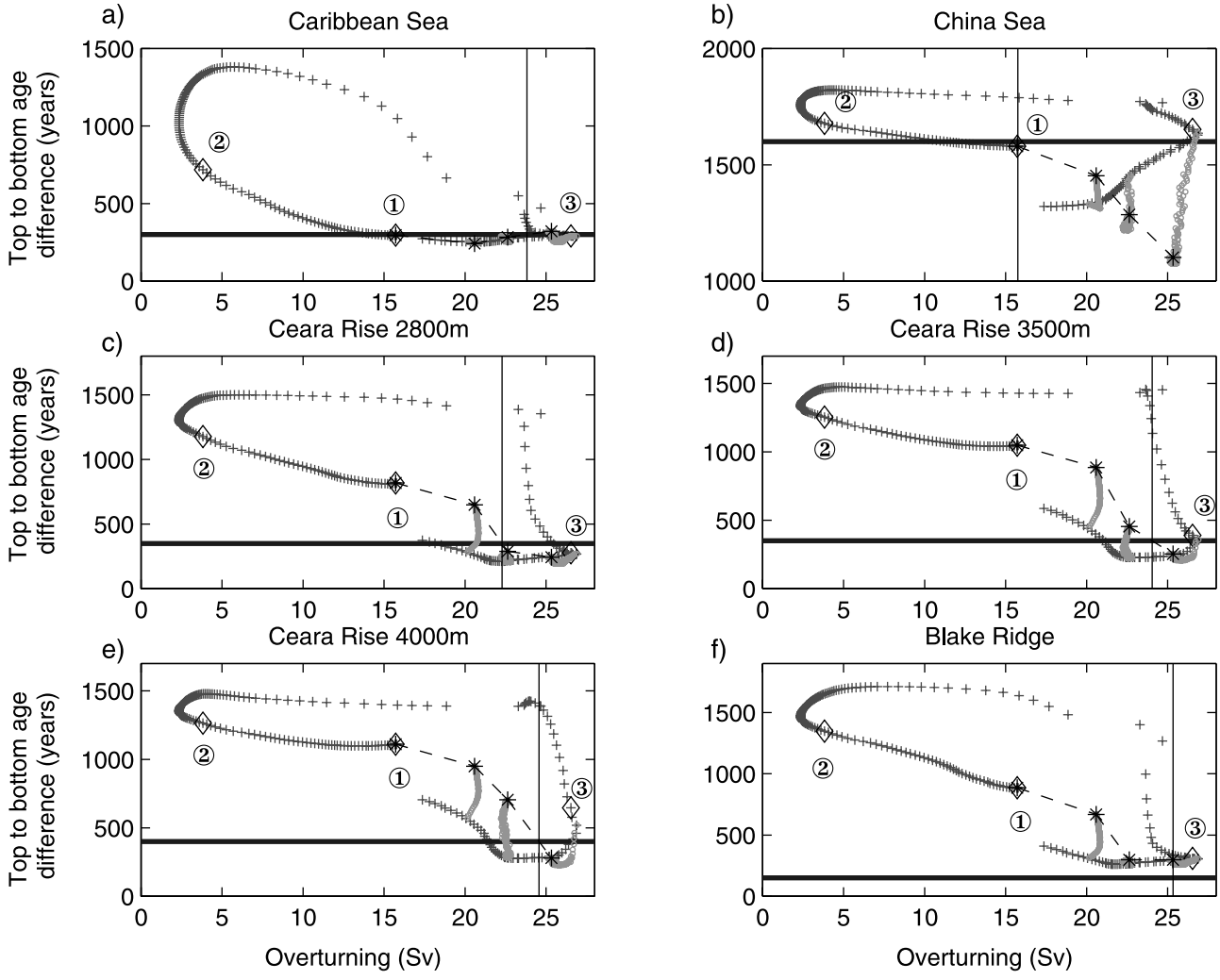

Figure 3. Top to bottom age difference (in years) as a function of the maximum strength of the meridional overturning (in Sv) for experiment PD FWP and the three equilibrium runs, compared to data from cores Vema 28-122 (a), Sonne 50-37KL (b), Knorr 110-82GGC (c), Knorr 110-66GGC (d), Knorr 110-50GGC (e) and Knorr 140-39GGC (f). Model results are annual means and plotted every ten integration years (red crosses for experiment PD FWP, green circles for the equilibrium runs). The black diamonds indicate the model results at points 1, 2 and 3 (end of the control run and maximum and minimum of freshwater forcing, respectively; see Figure 1). The results of the control run and the three equilibrium runs are represented by black stars. The sediment core data for the Holocene (core tops) are represented by the thick blue line (*Broecker et al.* [1990b], Caribbean Sea (a), South China Sea (b), Ceara Rise (c, d, e) and [*Keigwin and Schlegel*, 2002], Blake Ridge (f)). The black dashed line indicates an interpolation between the three equilibrium runs and the PD control run. Its intersection with sediment core data shows the overturning strength in the model which fits best with observations (vertical lines; for South China Sea and Blake Ridge, the vertical line indicates the minimum distance between the interpolation and observations). See color version of this figure at back of this issue.

specific humidity as described by *Weaver et al.* [2001]. The wind stress at the ocean surface as well as the wind fields used for moisture advection are the same for present-day and LGM runs, respectively. Diffusion occurs along and across isopycnals and a parameterization of the effect of mesoscale eddies on the tracer distribution is included [*Gent and McWilliams*, 1990]. Mixing parameters are the same for LGM and PD simulations. The location and rates of deep water formation are realistic in our model as has been validated with CFC concentrations [*Saenko et al.*, 2002]. A general overview of efforts to validate and diagnose ocean models by incorporating geochemical tracers as prognostic variables is given by *England and Maier-Reimer* [2001].

[9] Radiocarbon is introduced as a passive tracer in the ocean model with a half-life of 5730 years [*Toggweiler et al.*, 1989]. During a present-day (PD) and an LGM control run the atmospheric $^{14}C/^{12}C$ ratio (called $^{14}C^{atm}/^{12}C$ hereafter) is held fixed to the preindustrial standard ratio. The

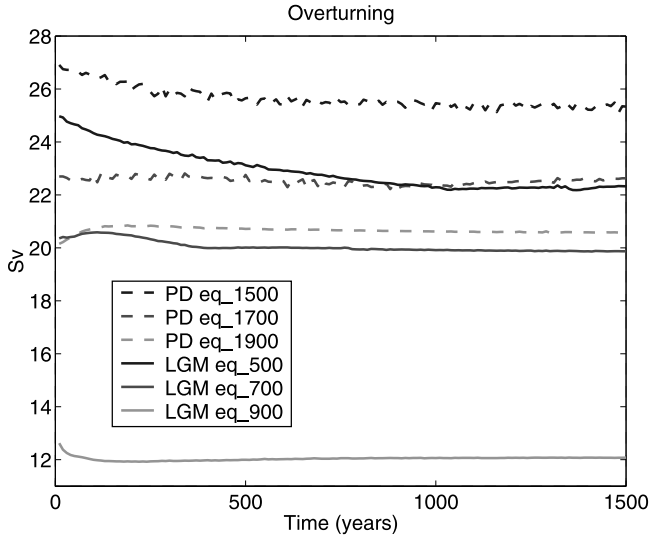

Figure 4. Time series of the maximum of the overturning motion for the equilibrium runs PD eq_1500 (blue dashed), PD eq_1700 (red dashed), PD eq_1900 (green dashed), LGM eq_500 (blue solid), LGM eq_700 (red solid) and LGM eq_900 (green solid) (see Figure 1). See color version of this figure at back of this issue.

air-sea exchange of radiocarbon is parameterized as in the work *Stocker and Wright* [1996, equation (A2)] with a restoring time τ equal to 5 years [see *Stocker and Wright*, 1996, and references therein].

[10] The two control experiments are then integrated for 3000 years to reach a quasi-equilibrium. At the end of the control runs, we diagnose the $^{14}C^{atm}$ production rates at the top of the atmosphere needed to keep the $^{14}C^{atm}/^{12}C$ ratio constant for the PD and the LGM scenarios, respectively. This procedure yields a production rate of 1.31 atoms/(cm^{2}s) for the PD run and 1.27 atoms/(cm^{2}s) for the LGM run. These production rates lie within the order of magnitude of other model-based estimates; *Masarik and Beer* [1999] simulate a present-day production rate varying spatially between 0.83 and 4.55 atoms/(cm^{2}s) (their global average amounts to 2.02 atoms/(cm^{2}s)).

[11] In order to simulate different overturning rates, perturbations of the surface freshwater fluxes in the North Atlantic are used. In these perturbation experiments (Exp PD FWP and LGM FWP), we apply the $^{14}C^{atm}$ production rates diagnosed at the end of the control runs to the atmosphere.

[12] We introduce a perturbation of freshwater fluxes into the North Atlantic (between 50°N and 70°N) at a rate of 0.6 Sv per 1000 years as in the work of *Schmittner et al.* [2002b]. The $^{14}C^{atm}/^{12}C$ ratio is then calculated prognostically and can respond to changes in the oceanic circulation and in the oceanic radiocarbon uptake due to the freshwater perturbation. By introducing the freshwater perturbation, the distribution of oceanic $^{14}C/^{12}C$ ratio (called $^{14}C^{ocn}/^{12}C$ hereafter) can be studied for various strengths of the North Atlantic overturning. We use these simulations to infer if age reversals are simulated in the deep ocean as observed by *Adkins et al.* [1998].

[13] In order to assess the overturning rate during the Last Glacial Maximum three additional experiments are conducted for LGM and PD boundary conditions, respectively (PD eq_1500, PD eq_1700, PD eq_1900 and LGM eq_500, LGM eq_700, LGM eq_900), during which the freshwater perturbation is kept constant for 1500 years in order to simulate near equilibrium distributions of radiocarbon for different rates of overturning (Figure 1). This approach is consistent with the notion that the overturning during the LGM was near equilibrium.

3. Results for Present-Day Simulations

[14] The introduction of a freshwater flux perturbation (experiments PD FWP and LGM FWP) in the northern North Atlantic leads to a hysteresis behavior of the meridional overturning, which is shown in Figure 2. Comparing the two hysteresis curves it can be seen that the LGM curve is narrower than the PD curve, indicating that the overturning is less stable under LGM than under PD conditions, consistent with earlier findings [*Schmittner et al.*, 2002b; *Ganopolski and Rahmstorf*, 2001].

[15] The evolution of the top to bottom age differences during the PD FWP and the three PD equilibrium runs are compared with sediment data at six locations in Figure 3. As the ocean model, with a resolution of 1.8° × 3.6°, has a necessarily coarse topography, we interpolated our data to the six locations and depths of sediment data for the comparative study. At all locations, the top to bottom age difference increases for a decreasing overturning (between points 1 and 2; red crosses in Figure 3). When the freshwater perturbation starts to decrease (after point 2; see Figure 1), the ocean does not react immediately, and the top to bottom age differences continue to increase while the overturning motion continues to decrease. A rapid transition toward smaller top to bottom age differences can be seen after the onset of the North Atlantic Deep Water (NADW) formation (before point 3), except in the China Sea where it is slower. The transient response of the modeled $^{14}C/^{12}C$ is the consequence of changes in the water masses which occupy the particular sites. As younger NADW is replaced by older Antarctic Bottom Water (AABW), the top to bottom age differences increase and vice versa.

[16] In order to get an idea about the $^{14}C/^{12}C$ distributions in an equilibrium state, we run three additional equilibrium runs (PD eq_1500, PD eq_1700, PD eq_1900) during which the freshwater forcing was kept constant for 1500 years (see Figure 1). Time series of the maximum meridional overturning in the North Atlantic as well as of the top to bottom age difference in the six studied locations can be seen in Figures 4 and 5, respectively. The results of these equilibrium runs are also reported as green circles in Figure 3; the final results after 1500 years of integration are marked by black stars. We then interpolate a response between the four equilibrium results (PD control run, PD eq_1500, PD eq_1700, PD eq_1900, all represented by black stars). This "equilibrium response" (represented by the black dashed line) shows a similar behavior in all locations except for the Caribbean Sea. Considering its slope, we can see that the sensitivity of radiocarbon to overturning is highly nonlinear.

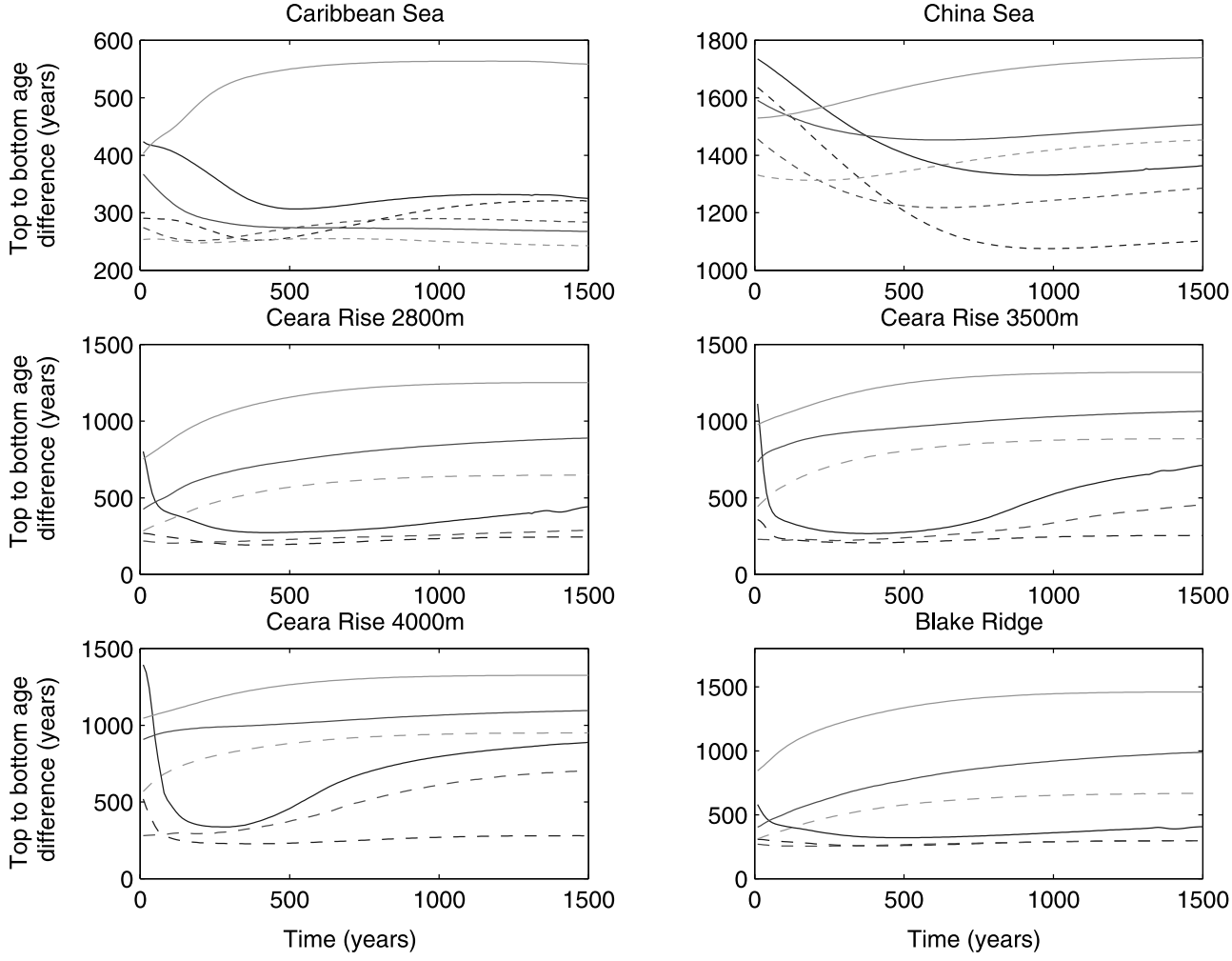

Figure 5. Time series of the top to bottom age differences (in years) at each of the six locations for the equilibrium runs PD eq_1500 (blue dashed), PD eq_1700 (red dashed) PD eq_1900 (green dashed), LGM eq_500 (blue solid), LGM eq_700 (red solid) and LGM eq_900 (green solid) (see Figure 1). See color version of this figure at back of this issue.

The top to bottom age difference varies more for high overturning rates (>20 Sv) than for intermediate overturning rates (<20 Sv). At the two shallower locations at the Ceara Rise as well as at the Blake Ridge, the top to bottom age difference varies less for very high overturning rates (when the advective time scale is very small; between PD eq_1500 and PD eq_1700). For the locations at the Ceara Rise, we can also see that the sensitivity at very high overturning rates increases with depth.

[17] The intersection of the ''equilibrium response'' (black dashed line) with the blue line (observations for the Holocene; core tops) gives the meridional overturning strength in best agreement with observations. The best fit with observations for the 5 locations in the North Atlantic is given for a meridional overturning strength between 22.3 and 25.3 Sv (23.8 Sv for the Caribbean Sea, 22.3 Sv, 24 Sv and 24.6 Sv for the Ceara Rise at 2800 m depth, 3500 m depth and 4000 m depth, respectively, and 25.3 Sv for the Blake Ridge). *Schmitz and McCartney* [1993] report a thermohaline transport of 18 Sv at 24°N. As ≃6 Sv recirculate within the North Atlantic in our model, 22–25 Sv is in excellent agreement with observed values of the present-day overturning.

[18] This success represents an independent validation of our method of finding the circulation strength from the ^{14}C distribution. Only the location in the South China Sea gets the best results for an overturning strength of 15.75 Sv. As the $^{14}C^{ocn}/^{12}C$ distribution in the Pacific is dominated by diffusion [*Toggweiler et al.*, 1989], the results in the South China Sea are not very relevant to measure the meridional overturning in the North Atlantic and might rather indicate errors in the value for the vertical diffusivity in the model.

[19] Out of the four equilibrium runs, PD eq_1700 with an overturning strength of 22.7 Sv is in best agreement with the sediment core data. A comparison between the $^{14}C^{ocn}/^{12}C$ ratio in PD eq_1700 and observed ^{14}C data from the Geochemical Ocean Sections Study (GEOSECS) (available at http://ingrid.ldgo.columbia.edu/SOURCES/.GEOSECS/) is shown in Figure 6. Contamination of oceanic waters by

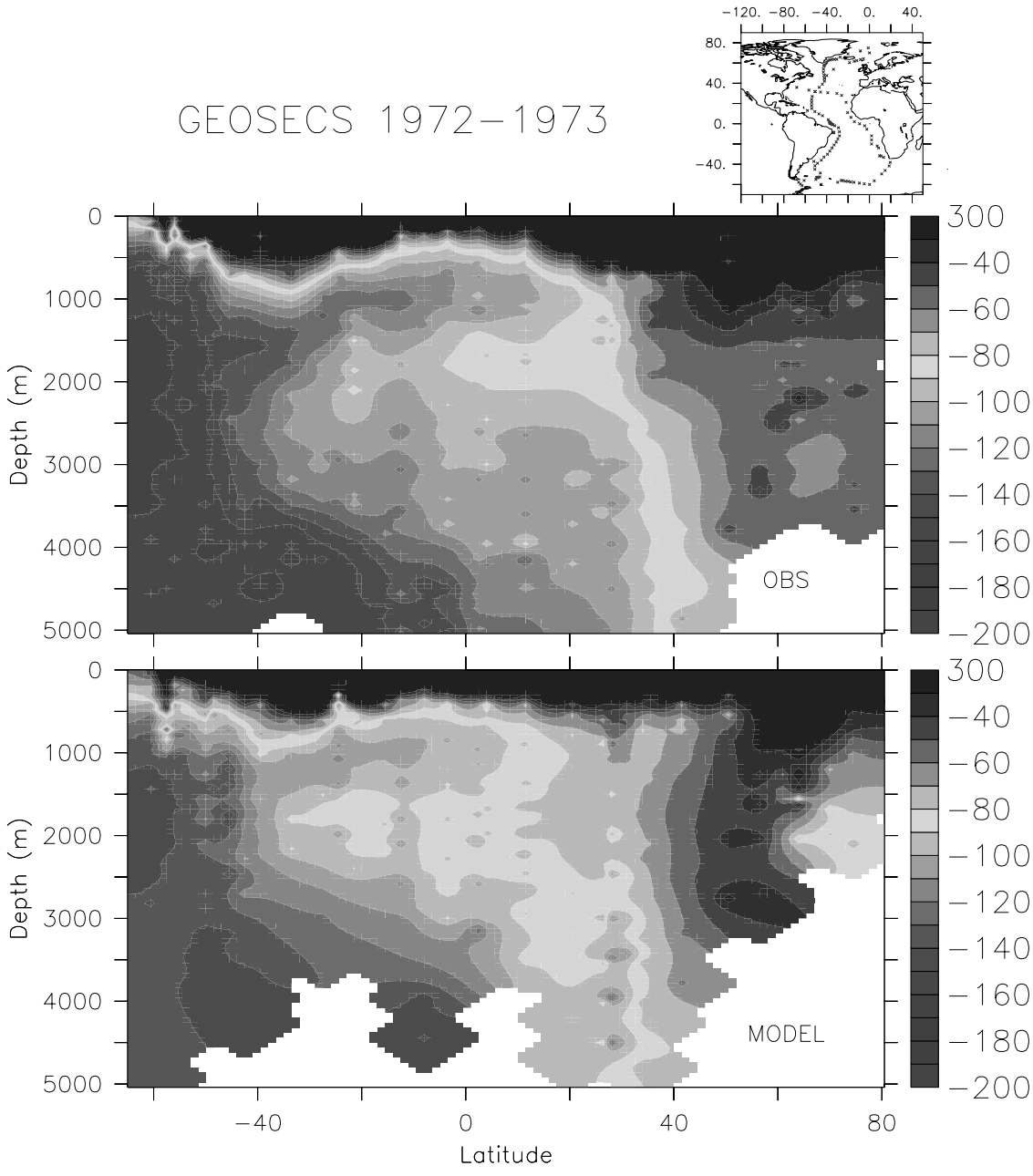

Figure 6. Distribution of the $^{14}C/^{12}C$ ratio (per mil) along the Atlantic sections of GEOSECS. The upper panel shows the location of data points, the middle panel observations (interpolation between the two sections), the lower panel model results from the PD eq_1700 run averaged over the years 1972–1973 (interpolation between the same grid points as for the observations). See color version of this figure at back of this issue.

the Suess effect and bomb ^{14}C were taken into account by prescribing a variable atmospheric $^{14}C/^{12}C$ ratio between 1840 and 1973 based on the industrial record [*Orr et al.*, 1999]. The simulated AABW in our PD equilibrium run has slightly higher $^{14}C/^{12}C$ ratios ($\simeq$140 per mil) than observed ($\simeq$160 per mil). This could lead to an underestimation of our top to bottom age differences in locations where younger water masses are replaced by AABW. NADW is well represented except for the deep Greenland Sea, where no trace of bomb ^{14}C can be seen. Overall, the simulated large scale structure of $^{14}C/^{12}C$ distribution shows the imprints of young NADW and the inflow of AABW similar to the observed data.

4. Results for Last Glacial Maximum Simulations

[20] The top to bottom age differences from LGM runs are shown in Figure 7. Starting with high age differences (point 1) the top to bottom age differences decrease with

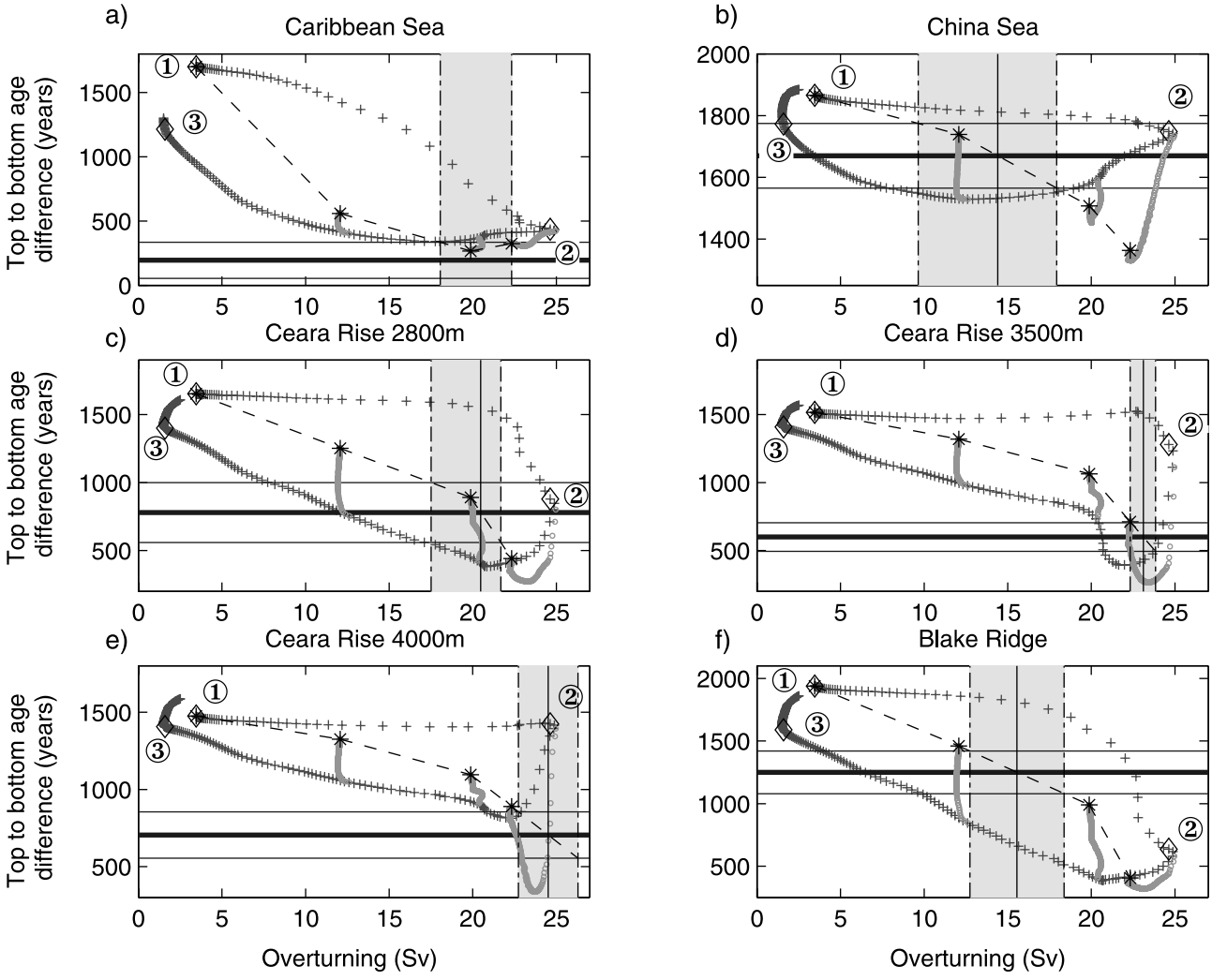

Figure 7. Top to bottom age difference (in years) as a function of the maximum strength of the meridional overturning (in Sv) for experiment LGM FWP and the three equilibrium runs compared to data from cores Vema 28-122 (a), Sonne 50-37KL (b), Knorr 110-82GGC (c), Knorr 110-66GGC (d), Knorr 110-50GGC (e) and Knorr 140-39GGC (f). Model results are annual means and plotted every ten integration years (red crosses for experiment LGM FWP, green circles for the equilibrium runs). The black diamonds indicate the model results at points 1, 2 and 3 (end of the control run and minimum and maximum freshwater forcing, respectively; see Figure 1). The results of the control run and the three equilibrium runs are represented by black stars. The sediment core data for the LGM are represented by the thick blue line, error bars by thin blue lines (*Broecker et al.* [1990b], Caribbean Sea (a), South China Sea (b), Ceara Rise (c, d, e) and [*Keigwin and Schlegel*, 2002], Blake Ridge (f)). The black dashed line indicates an interpolation between the three equilibrium runs and the LGM control run. Its intersection with the sediment core data (vertical lines) and its error bars (dash-dotted vertical lines) shows the range of overturning strength in the model which fits best with observations (yellow shaded). See color version of this figure at back of this issue.

increasing overturning (between point 1 and point 2, red crosses) during our LGM FWP run. When the freshwater perturbation in the North Atlantic starts to increase again (point 2), the overturning strength decreases. However, the advection of NADW is still strong enough to lead to a further decrease of top to bottom age differences at every location (after point 2). Finally, the overturning strength decreases enough to cause an increase in top to bottom age differences (before point 3). As in the present-day run these transient changes are caused by water masses of different radiocarbon concentrations flushing the sites.

[21] As for Figure 3, the results of our equilibrium runs (LGM control run, LGM eq_500, LGM eq_700 and LGM eq_900; see also Figures 4 and 5) are represented by black stars in Figure 7 and used to find the ''equilibrium response'' of the system (black dashed line). The intersec-

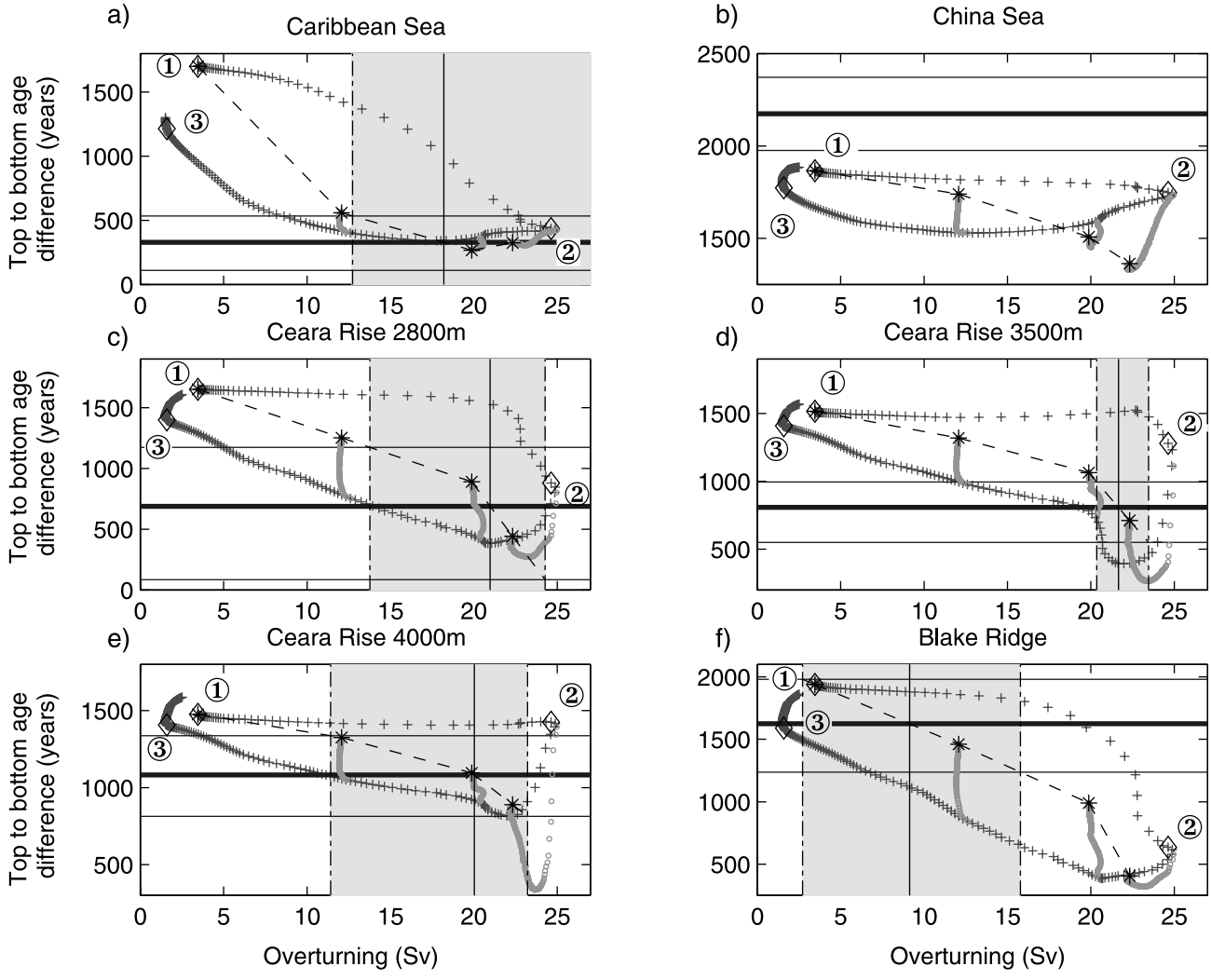

Figure 8. As Figure 7. Simulated top to bottom age difference (in years) are compared with redated data [*Adkins and Boyle*, 1997] assuming a reservoir age of 400 years. See color version of this figure at back of this issue.

tion of the "equilibrium response" with the measured data for the LGM (thick horizontal blue line), as well as with its error bars (thin horizontal blue lines), gives us an estimate of the overturning which is in best agreement with observations (yellow shaded area). The results for the Caribbean Sea and the three locations on the Ceara Rise are remarkably consistent; all indicate a very high overturning in best agreement with sediment data. Sediment data from South China Sea and Blake Ridge fit best with model results for a weakened overturning motion (~15 Sv).

[22] Measuring paleoocean ventilation by dating pairs of benthic and planktonic foraminifera requires a large number of specimens for analysis. Bioturbation [*Broecker et al.*, 1999] or sample contamination may lead to underestimates of the ventilation age where the sedimentation rates are low [*Broecker et al.*, 1999; *Keigwin and Schlegel*, 2002]. Very high sedimentation rates as well as dated peaks in flux of benthic foraminifera make data from the Blake Ridge more reliable than data from other sites in the North Atlantic. By this logic, we find the best agreement between model results and sediment data for an overturning between 12.7 and 18.3 Sv (Blake Ridge).

[23] The traditional calculation method for benthic-planktonic ventilation ages can be biased by changes in the atmospheric $^{14}C/^{12}C$ ratio. *Adkins and Boyle* [1997] develop a projection age method to avoid this problem. Using a reconstruction of atmospheric $^{14}C/^{12}C$ ratios, age differences based on bottom ^{14}C and atmospheric ^{14}C can be calculated. A 400-year reservoir age correction is introduced to account for the difference between atmospheric and surface ocean $^{14}C/^{12}C$ ratios [*Broecker et al.*, 1990a; *Adkins and Boyle*, 1997]. Sediment data from the Blake Ridge [*Keigwin and Schlegel*, 2002] are recalculated with this method. For the present study, we also redate the data from the Ceara Rise and the Caribbean Sea using this method. Data from the South China Sea are already redated by *Adkins and Boyle* [1997]. Model results compared with redated sediment data (and assuming a 400-year reservoir age correction) are shown in Figure 8. For the Atlantic cores, the most likely overturning strength is slightly weaker than for the comparison with

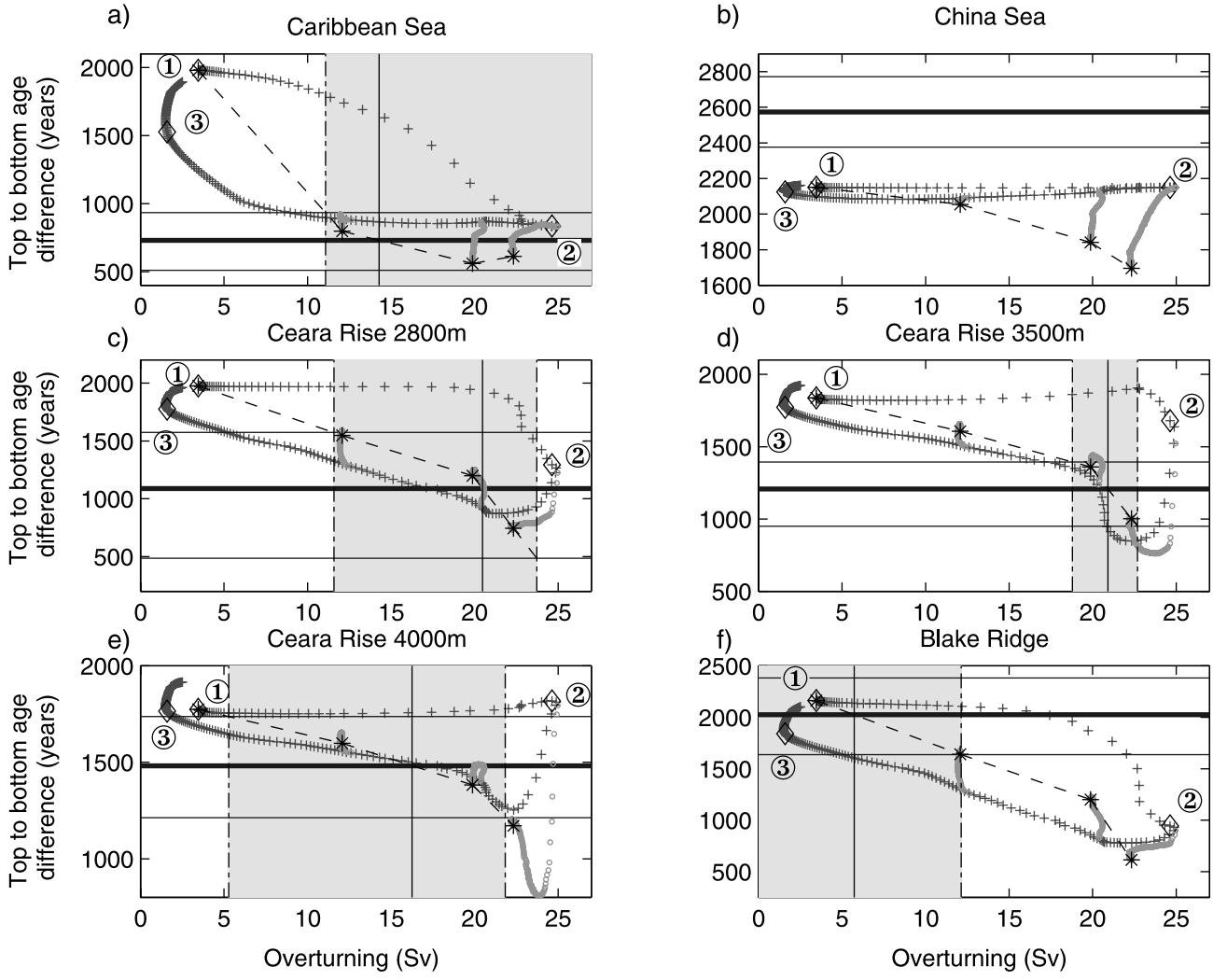

Figure 9. As Figure 7. Simulated atmospheric to bottom age difference (in years) are compared with redated data [*Adkins and Boyle*, 1997] (without reservoir age correction). See color version of this figure at back of this issue.

conventional top to bottom ages (Figure 7). At the Blake Ridge, the best fit indicates overturning strengths between 2.7 and 15.8 Sv.

[24] Surface $^{14}C/^{12}C$ distributions in the present ocean are not homogeneous. The assumption that the glacial ocean was characterized by a fixed reservoir age can be debated. As atmospheric $^{14}C/^{12}C$ ratios are calculated prognostically in our model runs, we complete our analysis with a third comparison between redated data (without reservoir age correction) and simulated atmospheric to bottom age differences. The results can be seen in Figure 9. Overall, the yellow areas indicate a further weakening of the most likely glacial circulation (0 to 12.1 Sv for the Blake Ridge).

[25] The simple parameterization of gas exchange between atmosphere and ocean in our model as well as the assumption of a fixed reservoir age leads to important uncertainties in the last two comparisons (Figures 8 and 9). On the other hand, redated ventilation ages for LGM and older events are highly uncertain because the INTCAL 98 calibration curve extends only to ~16.6 kyr BP. Beyond that there are only a few pairs of dates on early deglacial and LGM corals [*Bard et al.*, 1998; *Keigwin and Schlegel*, 2002]. The large error envelope around the calibration line leads to a further uncertainty of ±390 years (not included in Figures 8 and 9). The projection age method used in the present study [*Adkins and Boyle*, 1997] is also only applicable for one unmixed water mass.

[26] Following these arguments, our first analysis comparing conventional top to bottom age differences with model results (Figure 7) is probably the most reliable.

5. Ventilation of the Glacial North Atlantic

[27] Although 4 out of 5 North Atlantic sediment cores indicate a high overturning motion (≥17 Sv; Caribbean Sea and Ceara Rise; see Figure 7) as the most likely circulation, sediment data from the Blake Ridge are characterized by higher sedimentation rates and seem to be more reliable than data from other locations in the North Atlantic. We conclude that the distribution of radiocarbon obtained with

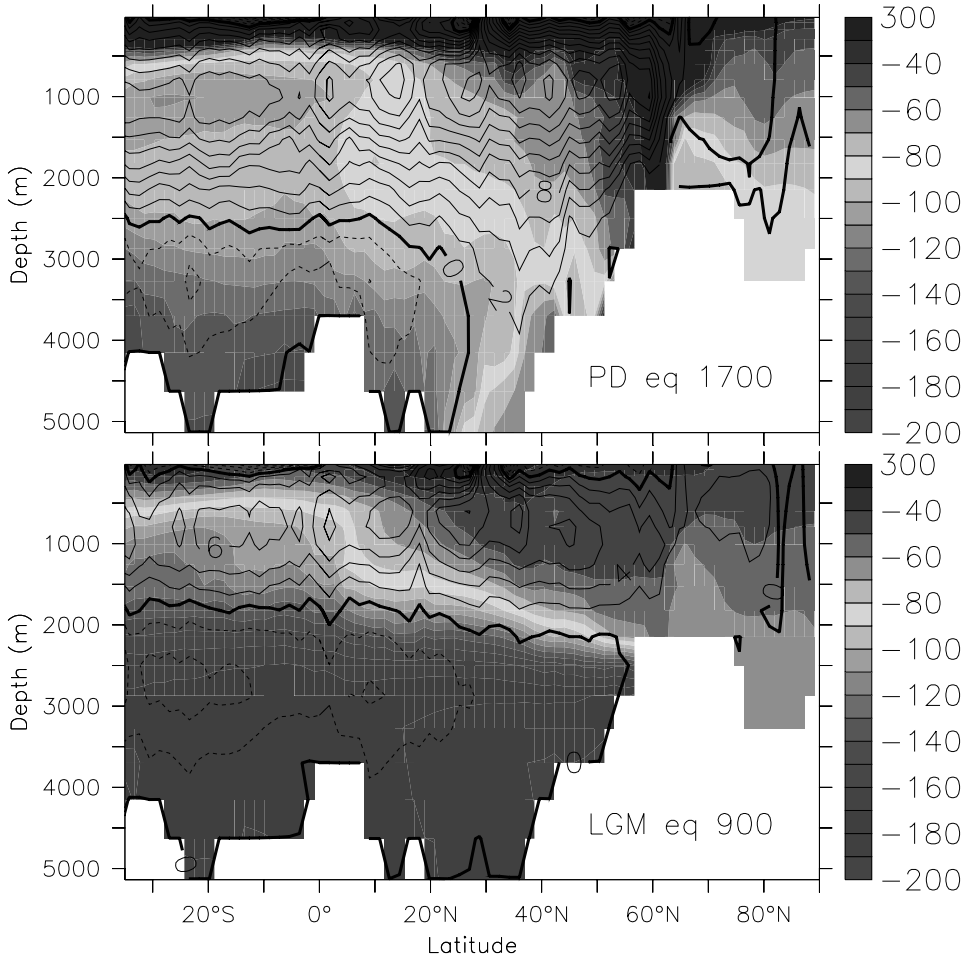

Figure 10. Distribution of the $^{14}C/^{12}C$ ratio (per mil), zonally averaged over the Atlantic. Isolines of the meridional stream function are represented as well. The upper panel shows annual means from the PD eq_1700 run, the lower panel annual means from the LGM eq_900 run. See color version of this figure at back of this issue.

an overturning weakened by 40% compared to today (core at Blake Ridge) is in best agreement with the sediment data. Our results are consistent with *Winguth et al.* [1999], who use nutrient distributions and report a 50% decreased circulation in best agreement with the observations. *Schmittner et al.* [2002a] compare six LGM equilibrium runs with overturning strengths varying from 4 Sv to 25 Sv, simulated by the same model we use for the present study, with sea surface temperature (SST) and sea surface salinity (SSS) data from *CLIMAP Project Members* [1981], *Seidov et al.* [1996] and *de Vernal et al.* [2000]. In that comparison, the highest correlation between simulated and reconstructed LGM minus PD Atlantic SST and SSS patterns is obtained for experiments with a shutdown or weak overturning motion.

[28] Equilibrium run LGM eq_900 with an overturning strength of 12 Sv is in best agreement with the sediment data. Its meridional stream function, as well as its zonal averaged $^{14}C/^{12}C$ ratio in the Atlantic, are compared to our best estimate for the present-day circulation (PD eq_1700) in Figure 10. Our analysis suggests that the thermohaline circulation was shallower during the LGM, leading to ^{14}C depleted water masses in the deep Atlantic Ocean. A strong gradient between water masses from northern and southern sources exists at 2000 m depth. For the PD simulation, the imprint of NADW and AABW can be seen in the $^{14}C/^{12}C$ ratio as in Figure 6. With the overlying isolines for the stream function, it is obvious that the tongue of ^{14}C depleted water at 1000–1500 m depth in the South Atlantic occurs in a region of small meridional advection while Antarctic Intermediate Water (AAIW) and NADW with higher $^{14}C/^{12}C$ ratios are present above and below, respectively.

6. Age Reversal Due to Water Mass Shifts

[29] Some results of LGM FWP at 38°N, 60°W and 1800 m depth show an interesting behavior. Between integration year 1100 and 1240, the water mass is replaced by older water at this location while the overturning is decreasing (Figure 11). This way the calendar age difference between these points equals 140 years, whereas the ^{14}C age difference of water between the same points is equal to 295.1 years. The biologically oldest part of an 140 year old deep sea coral growing at this location between integration year

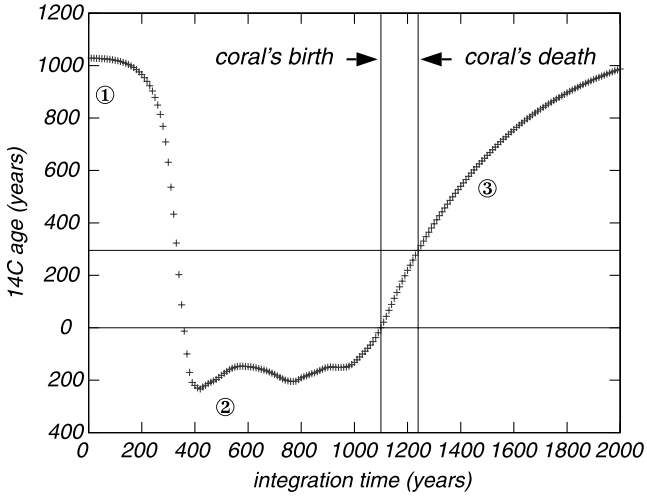

Figure 11. ^{14}C age (t) $-$ ^{14}C age (t = 1100) at 38°N, 60°W and 1800 m depth during the LGM FWP experiment (red crosses). The results are shown every 10 integration years. The fictive deep sea coral grows between the points indicated by horizontal and vertical lines. Points 1, 2 and 3 indicate the end of the control run, and the minimum and maximum of freshwater forcing, respectively (see Figure 1). See color version of this figure at back of this issue.

1100 and 1240 would be 295.1 years younger than its biologically youngest part in terms of ^{14}C age.

[30] This phenomenon of an ''age reversal'' was found in three deep sea corals at the same location by *Adkins et al.* [1998]. These corals of nearly the same depth (1800 m) lived 15,400 ± 150 years ago near the vertical boundary between glacial North Atlantic intermediate/deep water and southern source water. Nutrient measurements in one of these corals confirm that this vertical boundary shifted during the coral's lifetime. *Adkins et al.* [1998] interpret the coral's age reversal to be caused by an increase of the meridional overturning motion and a replacement of young glacial North Atlantic intermediate/deep water with older intermediate water of southern origin. In our model, an age reversal only occurs for a shutdown of the overturning, suggesting a rapid reduction of NADW, rather than an increase as recorded by *Adkins et al.* [1998]. The largest ^{14}C age difference (670 ± 60 years) found in a coral with a lifetime of 30 to 140 years is twice as large as the value simulated by the model. However, we should keep in mind that the simulated change is sensitive to the variation rate of the North Atlantic freshwater perturbation. Another reason for the discrepancy could be related to the coarse resolution of the model as well as the necessarily diffusive character of boundary currents, which underestimates gradients associated with narrow boundary currents and sharp fronts.

7. Uncertainties

[31] *Toggweiler et al.* [1989] carry out several experiments with different values of the vertical diffusion coefficient for heat, salt and tracers and different formulations for the gas exchange between atmosphere and ocean. According to their results, ^{14}C distributions depend strongly on the expression of vertical diffusion, whereas the spatial dependence of gas exchange is a second-order effect for deepwater ^{14}C. In the present study, the Gent/McWilliams scheme [*Gent and McWilliams*, 1990] is used. Whereas the overall simulated ^{14}C distribution is similar to observations (Figure 6), our AABW is slightly too young. By the same token, the simulated top to bottom age difference for the PD FWP run in the South China Sea (Figure 3) is too young to be consistent with the most likely PD overturning strength of between 22 and 25 Sv. In our LGM FWP runs the simulated top to bottom age differences in the South China Sea are always younger than the observations. This suggests that the diffusivity in our model is probably too large and that our top to bottom age differences in the Atlantic for a collapsed circulation might be also slightly underestimated. In better ventilated basins, however, vertical diffusion is less important and therefore uncertainties in diffusion coefficients are less likely to affect our results for active deep water circulation.

[32] The LGM FWP experiment is run with a constant $^{14}C^{atm}$ production rate which is diagnosed from the atmospheric ^{14}C budget at the end of the LGM control run. According to this approach, the diagnosed production is directly proportional to the atmospheric ^{14}C activity prescribed for the spin-up. During the LGM control run, ^{14}C is restored to a preindustrial value of 0 per mil. As estimates of the atmospheric $^{14}C/^{12}C$ ratio during the LGM reach 300 to 500 per mil [*Beck et al.*, 2001], a significantly higher $^{14}C^{atm}$ production rate would be diagnosed with a ''glacial'' value of $^{14}C^{atm}/^{12}C$ used during the spin-up. This discrepancy could lead to different results during transient experiments, because the surface and deep ocean $^{14}C/^{12}C$ ratio may not adjust at the same rate to a transient circulation change. If we consider the top to bottom age difference in equilibrium runs, however, the mean error in the $^{14}C^{atm}$ production rate vanishes.

[33] As already mentioned in section 3, another uncertainty is related to the sediment core data itself. *Broecker et al.* [1999] discuss the dangers in using benthic-planktonic foraminiferal age differences to reconstruct the radiocarbon age of late glacial deep ocean water. Gradients in the ratio of the planktonic foraminifera abundance to that of the benthics, as well as inter-species differences in the ^{14}C ages can lead to false results. As an alarming example, they mention the Holocene section of a sediment core taken at the Ceara Rise. In the case of the LGM section of the Caribbean core used in this study, different planktonic species gave very different ages [*Broecker et al.*, 1990b]. The sediment core from Blake Ridge [*Keigwin and Schlegel*, 2002] with high sedimentation rates circumvent some of these problems.

[34] It would be interesting to repeat the present study with a more accurate formulation for the gas exchange [e.g., *Siegenthaler*, 1983]. Experiments using both formulations show only minor differences as long as the atmospheric partial pressure of CO_2 is held constant [*Stocker and Wright*, 1996]. The introduction of a carbon cycle in our climate model is desirable as it would allow for the prediction of atmospheric partial pressures of CO_2 and calculation of gas exchange rate more accurately.

[35] During experiment LGM FWP the $^{14}C^{atm}/^{12}C$ ratio varies by 40 per mil which is slightly smaller than changes

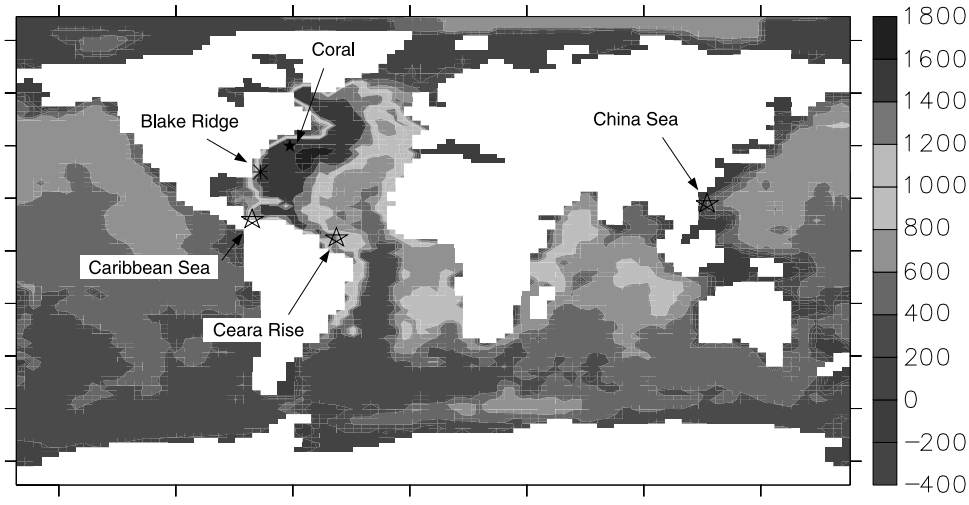

Figure 12. Difference between two extreme states (LGM control run (weak overturning) minus LGM eq_500 (strong overturning)) of the top to bottom age difference. The locations of the sea sediment cores and the deep sea coral are represented as well. See color version of this figure at back of this issue.

found in sediment cores (e.g., 50–70 per mil at the onset of the Younger Dryas) [*Hughen et al.*, 1998]. However, the variability of the $^{14}C^{atm}$ production rate, as well as changes in the carbon uptake of the biosphere, both not considered here, can have a crucial influence on the $^{14}C^{atm}/^{12}C$ ratio [*Marchal et al.*, 2001].

[36] Our study is limited by the small number of measurements available and would benefit greatly from a more spatially extensive proxy record. Particularly, more measurements from intermediate levels in the North Atlantic would be useful to determine the ventilation at shallower depths [*Marchitto et al.*, 1998]. According to our simulations, the largest impact on glacial top to bottom age differences due to changing overturning rates can be expected in sediments located west of the Mid-Atlantic Ridge in the Sargasso Sea, near the Bermuda Rise and as far north as the Labrador Sea (see Figure 12).

8. Conclusion

[37] Measured ^{14}C age differences between surface and deep waters provide powerful constraints on past ocean ventilation rates. In conjunction with simulations it is possible to estimate deep water formation rates, a quantity which is very difficult to infer with other methods. Our study suggests that deep water formation rates in the North Atlantic reduced by about 40% compared to the present are consistent with available deep sea radiocarbon ages. However, we cannot exclude other circulation patterns (like an increase in AABW) to account for the observed radiocarbon distribution as suggested by *Wunsch* [2003]. We have also shown that age reversals in the North Atlantic found in deep sea corals [*Adkins et al.*, 1998] are simulated in our experiments. Contrary to the original interpretation of these observations by *Adkins et al.* [1998], however, our study suggests an abrupt reduction in deep water ventilation as the cause of the age reversal, rather than a rapid resumption of deep water production.

[38] **Acknowledgments.** We would like to thank Lloyd D. Keigwin for providing his submitted manuscript and for his useful comments about the interpretation of his data. Two anonymous reviewers and Matthew England were extraordinarily helpful with an earlier version of this paper. Furthermore, we would like to thank Carl Wunsch for many useful comments on an earlier version of this manuscript. Michael Eby's technical support was very appreciated. We are grateful for research grant support under the NSERC Operating, Strategic, CSHD and CFCAS research grant programs. Dáithí A. Stone is gratefully acknowledged for editing English grammar.

References

Adkins, J. F., and E. A. Boyle, Changing atmospheric $\Delta^{14}C$ and the record of deep water paleoventilation ages, *Paleoceanography*, *12*(3), 337–344, 1997.

Adkins, J. F., H. Cheng, E. A. Boyle, E. R. M. Druffel, and R. L. Edwards, Deep-sea coral evidence for rapid change in ventilation of the deep North Atlantic 15,400 years ago, *Science*, *280*, 725–728, 1998.

Bard, E., M. Arnold, B. Hamelin, N. Tisnerat-Laborde, and G. Cabioch, Radiocarbon calibration by means of mass spectrometric $^{230}Th/^{234}U$ and ^{14}C ages of corals: An updated database including samples from Barbados, Mururoa and Tahiti, *Radiocarbon*, *40*, 1085–1092, 1998.

Beck, J. W., et al., Extremely large variations of atmospheric ^{14}C concentration during the last glacial period, *Science*, *292*, 2453–2458, 2001.

Bitz, C. M., M. M. Holland, A. J. Weaver, and M. Eby, Simulating the ice-thickness distribution in a coupled climate model, *J. Geophys. Res.*, *106*, 2441–2464, 2001.

Boyle, E., Last-Glacial-Maximum North Atlantic Deep Water: On, off or somewhere in-between?, *Philos. Trans. R. Soc. London*, *348*, 243–253, 1995.

Boyle, E., and Y. Rosenthal, Chemical hydrography of the South Atlantic during the Last Glacial Maximum: Cd vs. $\delta^{13}C$, in *The South Atlantic: Present and Past Circulation*, edited by G. Wefer et al., pp. 423–443, Springer-Verlag, New York, 1996.

Broecker, W. S., M. Klas, E. Clark, S. Trumbore, G. Bonani, W. Wolfli, and S. Ivy, Accelerator mass spectrometric measurements on foraminifera shells from deep sea cores, *Radiocarbon*, *32*, 119–133, 1990a.

Broecker, W. S., T.-H. Peng, S. Trumbore, G. Bonani, and W. Wolfli, The distribution of radiocarbon in the glacial ocean, *Global Biogeochem. Cycles*, *4*, 103–106, 1990b.

Broecker, W. S., K. Matsumoto, E. Clark, I. Hajdas, and G. Bonani, Radiocarbon age differences between coexisting foraminiferal species, *Paleoceanography*, *14*(4), 431–436, 1999.

CLIMAP Project Members, Seasonal reconstructions of the earth's surface at the Last Glacial Maximum, *Map Chart Ser. MC-36*, Geol. Soc. Am., Boulder, Colo., 1981.

de Vernal, A., C. Hillaire-Marcel, J.-L. Turon, and J. Matthiessen, Reconstruction of sea-surface temperature, salinity and sea ice cover in the northern North Atlantic during the Last Glacial Maximum based on dinocyst assemblages, *Can. J. Earth Sci.*, *37*, 725–750, 2000.

Duplessy, J. C., L. Labeyrie, M. Paterne, S. Hovine, T. Fichefet, J. Duprat, and M. Labracherie, High latitude deep water sources during the Last Glacial Maximum and the intensity of global ocean circulation, in *The South Atlantic: Present and Past Circulation*, edited by G. Wefer et al., pp. 445–460, Springer-Verlag, New York, 1996.

England, M. H., and E. Maier-Reimer, Using chemical tracers to assess ocean models, *Rev. Geophys.*, *39*, 29–70, 2001.

Fichefet, T., S. Hovine, and J. C. Duplessy, A model study of the atlantic thermohaline circulation during the Last Glacial Maximum, *Nature*, *372*(6503), 252–255, 1994.

Ganopolski, A., and S. Rahmstorf, Rapid changes of glacial climate simulated in a coupled climate model, *Nature*, *409*, 153–158, 2001.

Gent, P. R., and J. C. McWilliams, Isopycnal mixing in ocean circulation models, *J. Phys. Oceanogr.*, *20*, 150–155, 1990.

Hughen, K. A., J. T. Overpeck, S. J. Lehman, M. Kashgarian, J. Southon, L. C. Peterson, R. Alley, and D. M. Sigman, Deglacial changes in ocean circulation from an extended radiocarbon calibration, *Nature*, *391*, 65–68, 1998.

Kalnay, E., et al., The NCEP/NCAR 40-year reanalysis project, *Bull. Am. Meteorol. Soc.*, *77*, 437–471, 1996.

Keigwin, L. D., and M. A. Schlegel, Ocean ventilation and sedimentation since the glacial maximum at 3 km in the western North Atlantic, *Geochem. Geophys. Geosyst.*, *3*(6), 1034, doi:10.1029/2001GC000283, 2002.

Lynch-Stieglitz, J., W. B. Curry, and N. Slowey, Weaker Gulf Stream in the Florida Straits during the Last Glacial Maximum, *Nature*, *402*(6762), 644–648, 1999.

Marchal, O., R. Francois, T. F. Stocker, and F. Joos, Ocean thermohaline circulation and sedimentary $^{231}Pa/^{230}Th$ ratio, *Paleoceanography*, *15*, 625–641, 2000.

Marchal, O., T. F. Stocker, and R. Muscheler, Atmospheric radiocarbon during the Younger Dryas: Production, ventilation, or both?, *Earth Planet. Sci. Lett.*, *185*, 383–395, 2001.

Marchitto, T. M., Jr., W. B. Curry, and D. L. Oppo, Millenial-scale changes in North Atlantic circulation since the last glaciation, *Nature*, *393*, 557–561, 1998.

Masarik, J., and J. Beer, Simulation of particle fluxes and cosmogenic nuclide production in the Earth's atmosphere, *J. Geophys. Res.*, *104*(D10), 12,099–12,111, 1999.

Meissner, K. J., and R. Gerdes, Coupled climate modelling of ocean circulation changes during ice age inception, *Clim. Dyn.*, *18*, 455–473, 2002.

Orr, J. C., R. Najjar, C. L. Sabine, and F. Joos, *Abiotic-HOWTO, Internal OCMIP Rep.*, 25 pp., Lab. des Sci. de Clim. et l'Environ., Comm. a l'Energie Atom., Saclay, Gif-sur-Yvette, France, 1999.

Pacanowski, R. C., MOM 2 Documentation, User's Guide and Reference Manual, *Tech. Rep. 3*, Geophys. Fluid Dyn. Lab. Ocean Group, Princeton, N. J., 1995.

Peltier, W. R., Ice age paleotopography, *Science*, *265*, 15–21, 1994.

Rutberg, R. L., S. R. Hemming, and S. L. Goldstein, Reduced North Atlantic Deep Water flux to the glacial Southern Ocean inferred from neodymium isotope ratios, *Nature*, *405*(6789), 935–938, 2000.

Saenko, O. A., A. Schmittner, and A. J. Weaver, On the role of wind-driven motion on ocean ventilation, *J. Phys. Oceangr.*, *32*(12), 3376–3395, 2002.

Schmittner, A., K. J. Meissner, M. Eby, and A. J. Weaver, Forcing of the deep ocean circulation in simulations of the Last Glacial Maximum, *Paleoceanography*, *17*(2), 1015, doi:10.1029/2001PA000633, 2002a.

Schmittner, A., M. Yoshimori, and A. J. Weaver, Instability of glacial climate in a model of the ocean-atmosphere-cryosphere system, *Science*, *295*, 1489–1493, 2002b.

Schmitz, W. J., and M. S. McCartney, On the North Atlantic circulation, *Rev. Geophys.*, *31*, 29–49, 1993.

Seidov, D., M. Sarnthein, K. Stattegger, R. Prien, and M. Weinelt, North Atlantic ocean circulation during the Last Glacial Maximum and subsequent meltwater event: A numerical model, *J. Geophys. Res.*, *101*, 16,305–16,332, 1996.

Siegenthaler, U., Uptake of excess CO_2 by an outcrop-diffusion model of the ocean, *J. Geophys. Res.*, *88*, 3599–3608, 1983.

Stocker, T. F., and D. G. Wright, Rapid changes in ocean circulation and atmospheric radiocarbon, *Paleoceanography*, *11*(6), 773–795, 1996.

Toggweiler, J. R., K. Dixon, and K. Bryan, Simulations of radiocarbon in a coarse-resolution world ocean model, 1, Steady state prebomb distributions, *J. Geophys. Res.*, *94*(C6), 8217–8242, 1989.

Weaver, A. J., M. Eby, A. F. Fanning, and E. C. Wiebe, Simulated influence of carbon dioxide, orbital forcing and ice sheets on the climate of the Last Glacial Maximum, *Nature*, *394*, 847–853, 1998.

Weaver, A. J., et al., The Uvic Earth System Climate Model: Model description, climatology, and applications to past, present and future climates, *Atmos. Ocean*, *4*, 361–428, 2001.

Winguth, A. M. E., D. Archer, J. C. Duplessy, E. Maier-Reimer, and U. Mikolajewicz, Sensitivity of paleonutrient tracer distributions and deepsea circulation to glacial boundary conditions, *Paleoceanography*, *14*, 304–323, 1999.

Wunsch, C., Determining paleoceanographic circulations, with emphasis on the Last Glacial Maximum, *Quat. Sci. Rev.*, *22*, 371–385, 2003.

Yu, E. F., R. Francois, and M. P. Bacon, Similar rates of modern and last-glacial ocean thermohaline circulation inferred from radiochemical data, *Nature*, *379*, 689–694, 1996.

J. F. Adkins, Geological and Planetary Sciences, California Institute of Technology, MS 100-23 1200, E. California Blvd., Pasadena, CA 91125, USA. (jess@gps.caltech.edu)

K. J. Meissner, A. Schmittner, and A. J. Weaver, School of Earth and Ocean Sciences, University of Victoria, PO Box 3055, Stn CSC, Victoria, BC V8W 3P6, Canada. (katrin@ocean.seos.uvic.ca; aschmit@bgc-jena.mpg.de; weaver@ocean.seos.uvic.ca)

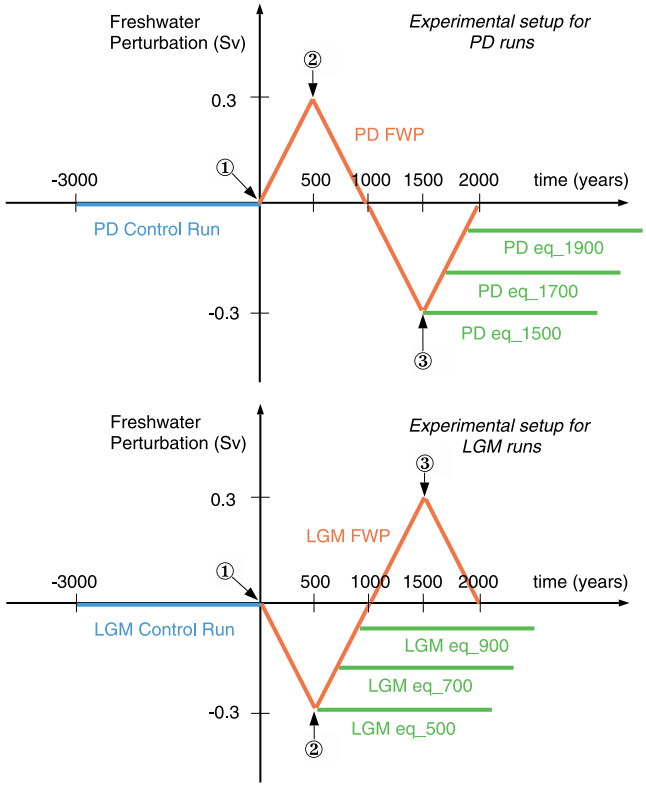

Figure 1. Schematic representation of the experimental design for PD and LGM runs, respectively. The control runs are represented in blue, the freshwater flux perturbation runs in red and the equilibrium runs in green. The points 1, 2 and 3 refer to Figures 2, 3, 7, 8, 9, and 11; 1 represents the end of the control runs and 2 and 3 the maxima and minima of the freshwater forcing.

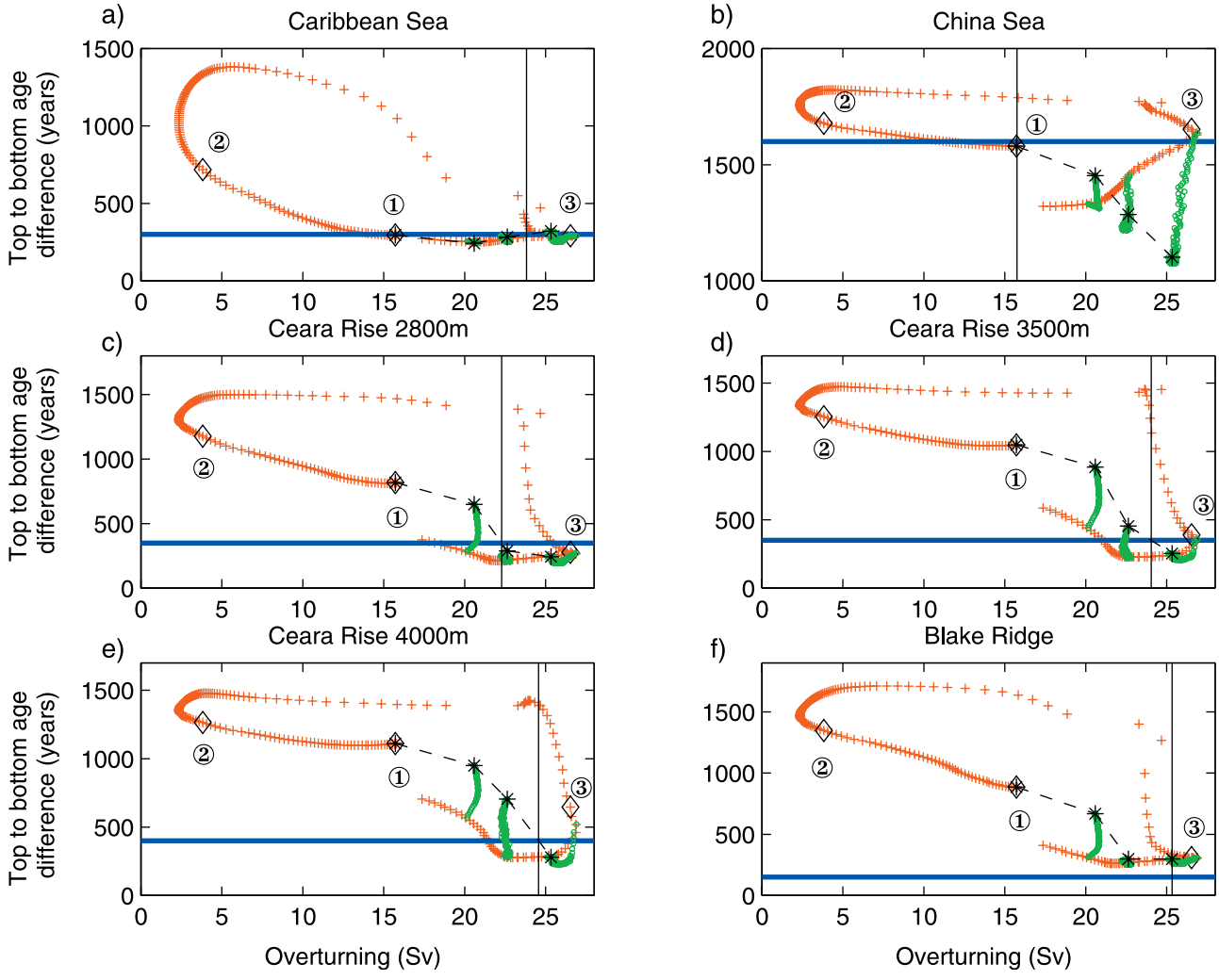

Figure 3. Top to bottom age difference (in years) as a function of the maximum strength of the meridional overturning (in Sv) for experiment PD FWP and the three equilibrium runs, compared to data from cores Vema 28-122 (a), Sonne 50-37KL (b), Knorr 110-82GGC (c), Knorr 110-66GGC (d), Knorr 110-50GGC (e) and Knorr 140-39GGC (f). Model results are annual means and plotted every ten integration years (red crosses for experiment PD FWP, green circles for the equilibrium runs). The black diamonds indicate the model results at points 1, 2 and 3 (end of the control run and maximum and minimum of freshwater forcing, respectively; see Figure 1). The results of the control run and the three equilibrium runs are represented by black stars. The sediment core data for the Holocene (core tops) are represented by the thick blue line (*Broecker et al.* [1990b], Caribbean Sea (a), South China Sea (b), Ceara Rise (c, d, e) and [*Keigwin and Schlegel*, 2002], Blake Ridge (f)). The black dashed line indicates an interpolation between the three equilibrium runs and the PD control run. Its intersection with sediment core data shows the overturning strength in the model which fits best with observations (vertical lines; for South China Sea and Blake Ridge, the vertical line indicates the minimum distance between the interpolation and observations).

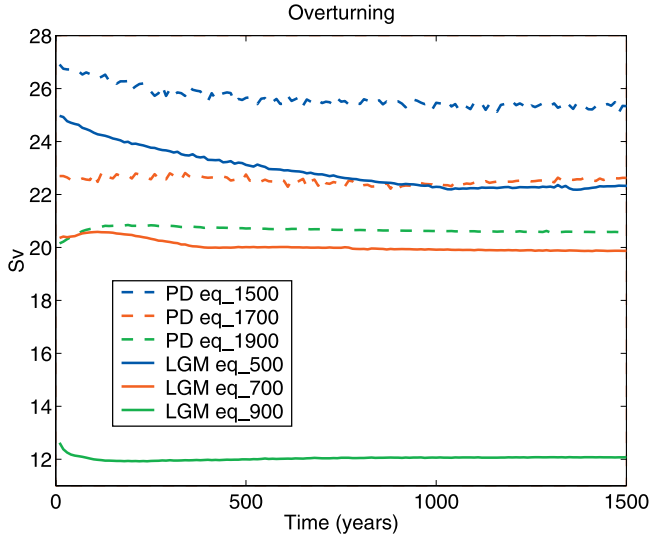

Figure 4. Time series of the maximum of the overturning motion for the equilibrium runs PD eq_1500 (blue dashed), PD eq_1700 (red dashed), PD eq_1900 (green dashed), LGM eq_500 (blue solid), LGM eq_700 (red solid) and LGM eq_900 (green solid) (see Figure 1).

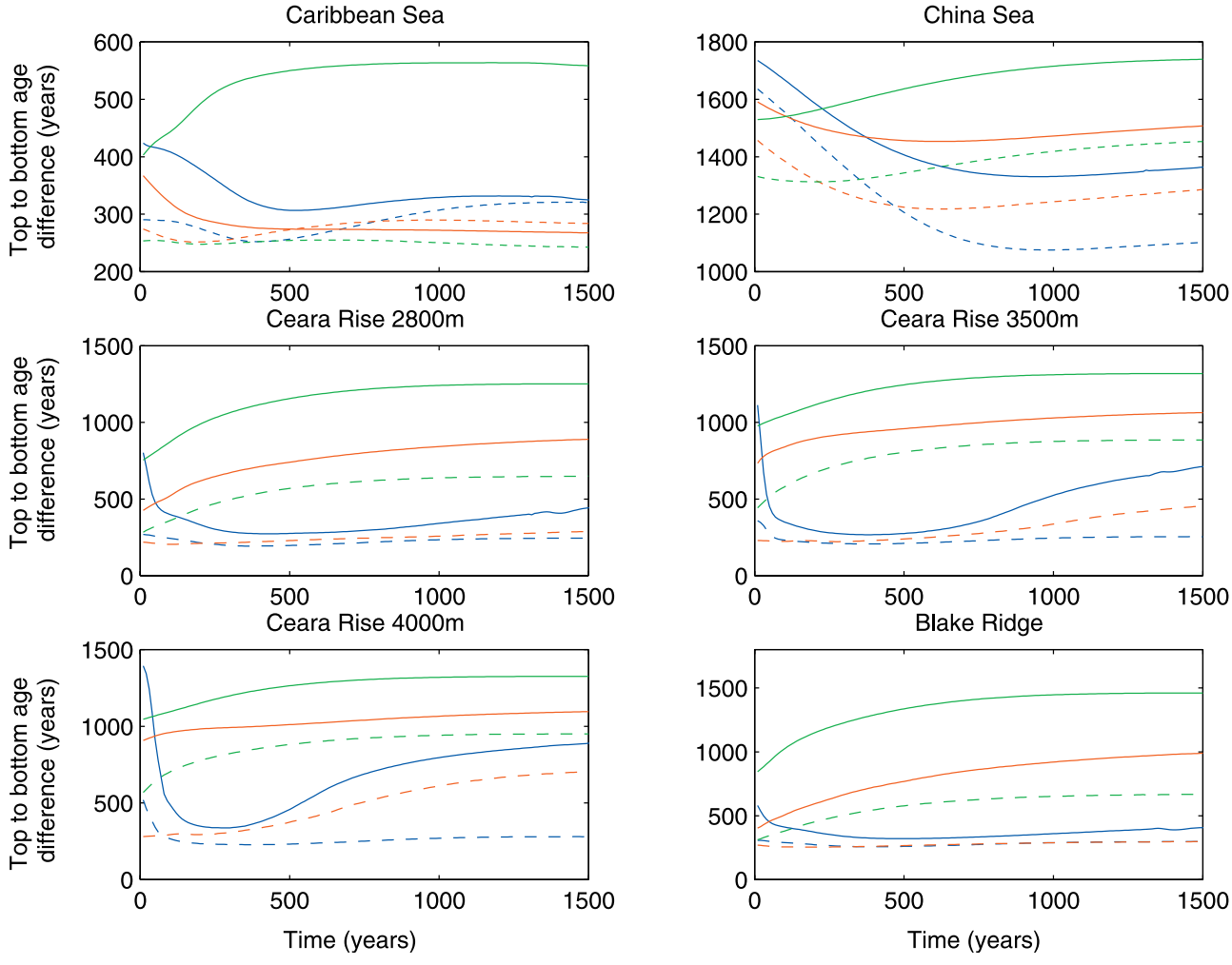

Figure 5. Time series of the top to bottom age differences (in years) at each of the six locations for the equilibrium runs PD eq_1500 (blue dashed), PD eq_1700 (red dashed) PD eq_1900 (green dashed), LGM eq_500 (blue solid), LGM eq_700 (red solid) and LGM eq_900 (green solid) (see Figure 1).

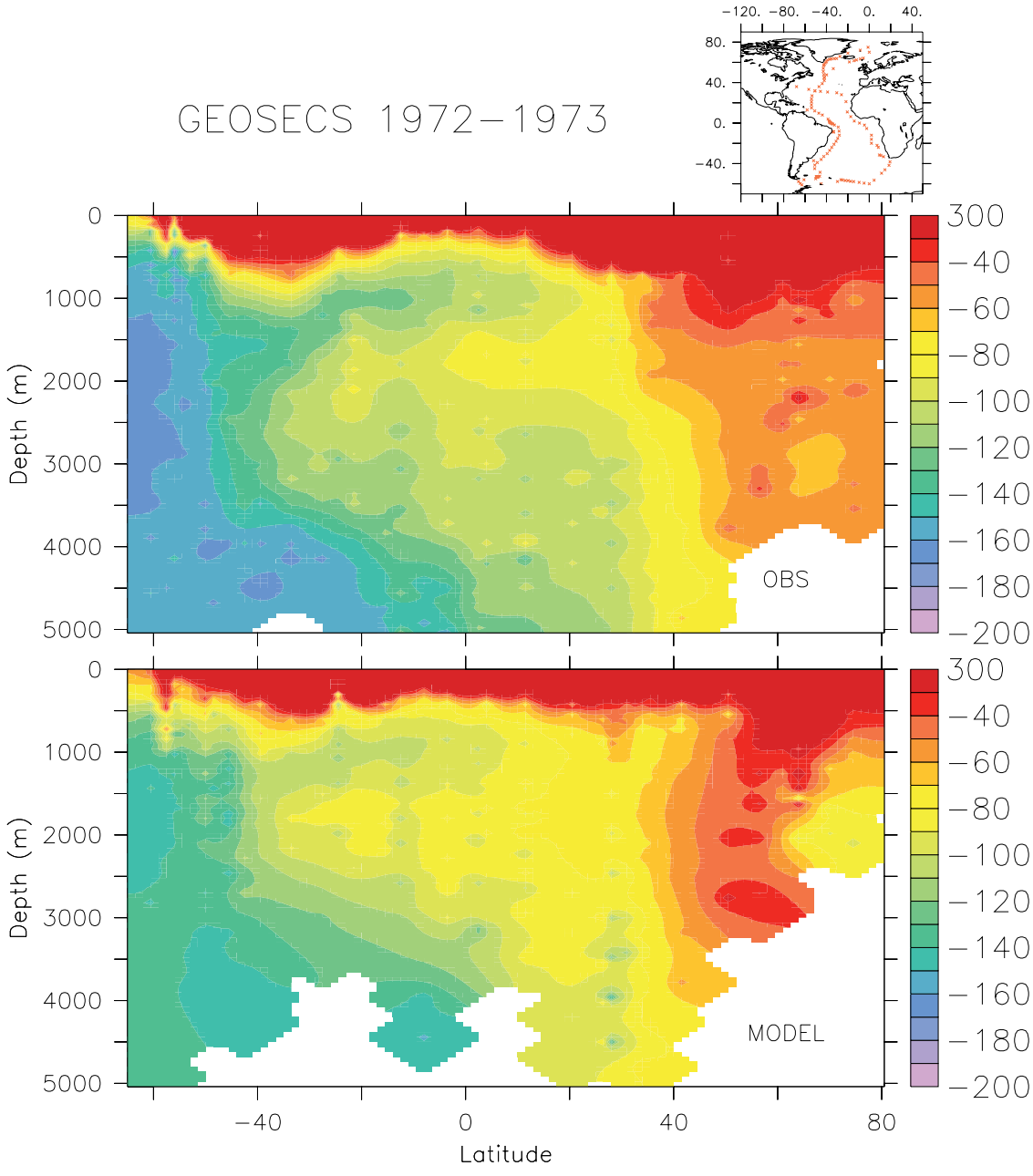

Figure 6. Distribution of the $^{14}C/^{12}C$ ratio (per mil) along the Atlantic sections of GEOSECS. The upper panel shows the location of data points, the middle panel observations (interpolation between the two sections), the lower panel model results from the PD eq_1700 run averaged over the years 1972–1973 (interpolation between the same grid points as for the observations).

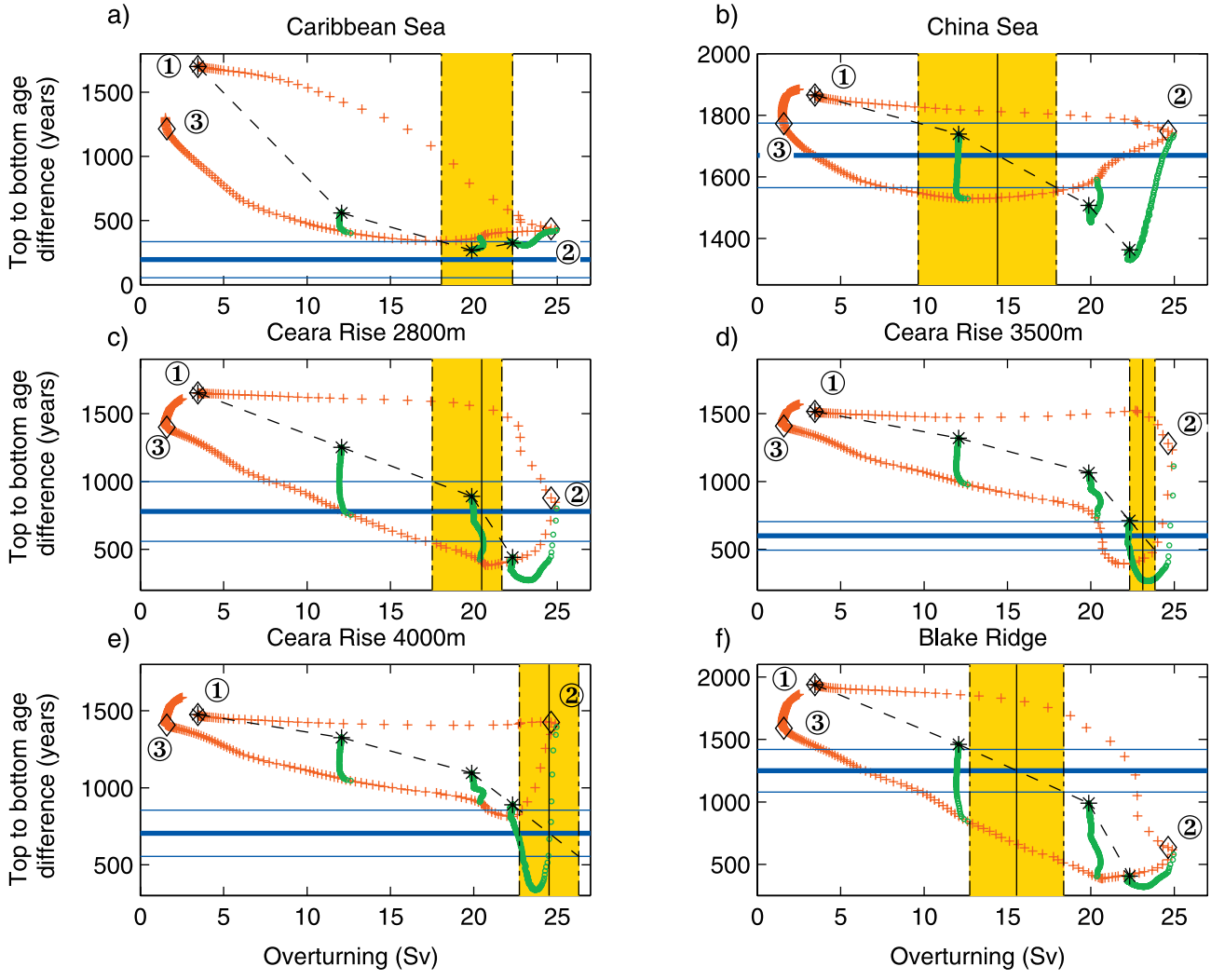

Figure 7. Top to bottom age difference (in years) as a function of the maximum strength of the meridional overturning (in Sv) for experiment LGM FWP and the three equilibrium runs compared to data from cores Vema 28-122 (a), Sonne 50-37KL (b), Knorr 110-82GGC (c), Knorr 110-66GGC (d), Knorr 110-50GGC (e) and Knorr 140-39GGC (f). Model results are annual means and plotted every ten integration years (red crosses for experiment LGM FWP, green circles for the equilibrium runs). The black diamonds indicate the model results at points 1, 2 and 3 (end of the control run and minimum and maximum freshwater forcing, respectively; see Figure 1). The results of the control run and the three equilibrium runs are represented by black stars. The sediment core data for the LGM are represented by the thick blue line, error bars by thin blue lines (*Broecker et al.* [1990b], Caribbean Sea (a), South China Sea (b), Ceara Rise (c, d, e) and [*Keigwin and Schlegel*, 2002], Blake Ridge (f)). The black dashed line indicates an interpolation between the three equilibrium runs and the LGM control run. Its intersection with the sediment core data (vertical lines) and its error bars (dash-dotted vertical lines) shows the range of overturning strength in the model which fits best with observations (yellow shaded).

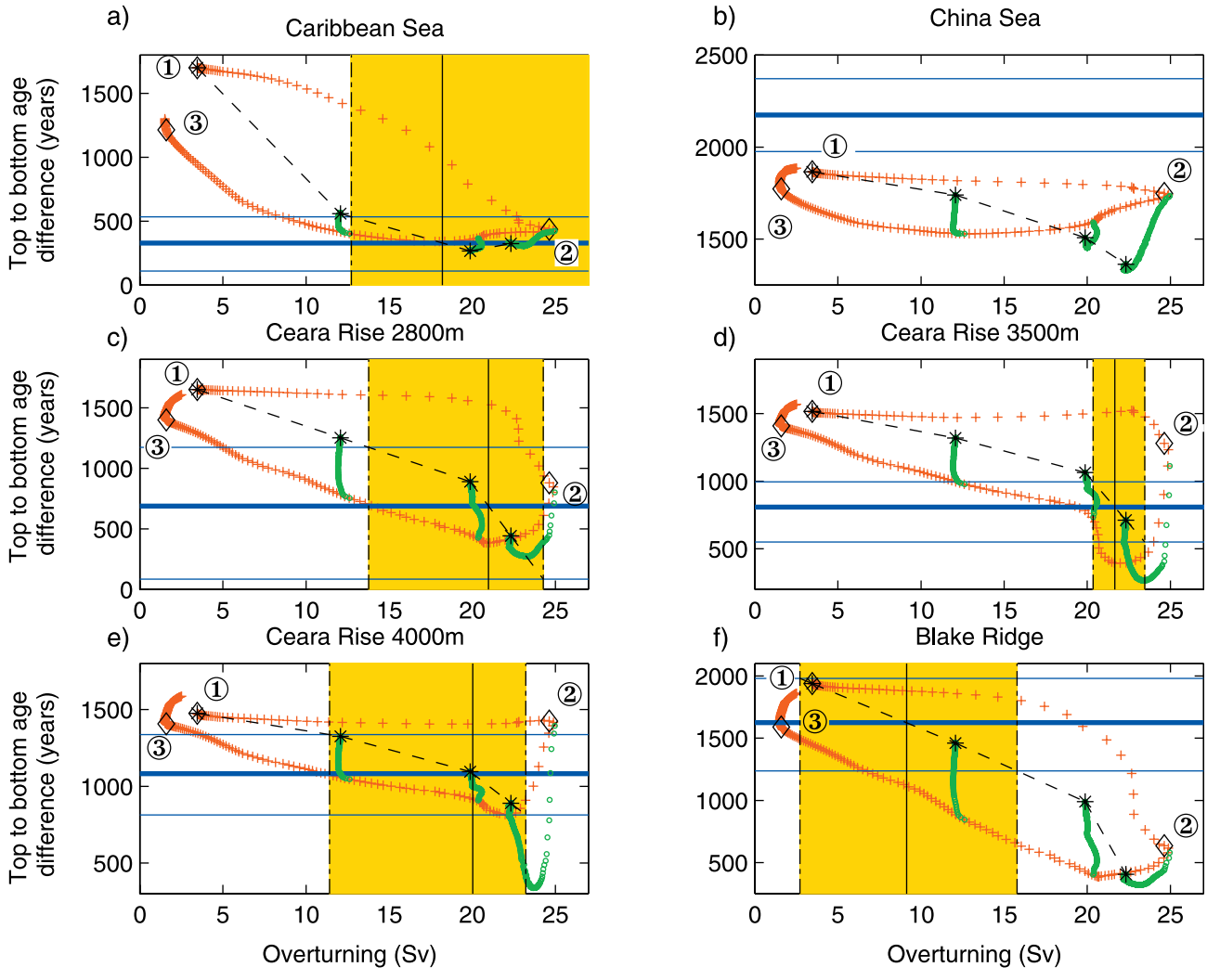

Figure 8. As Figure 7. Simulated top to bottom age difference (in years) are compared with redated data [*Adkins and Boyle*, 1997] assuming a reservoir age of 400 years.

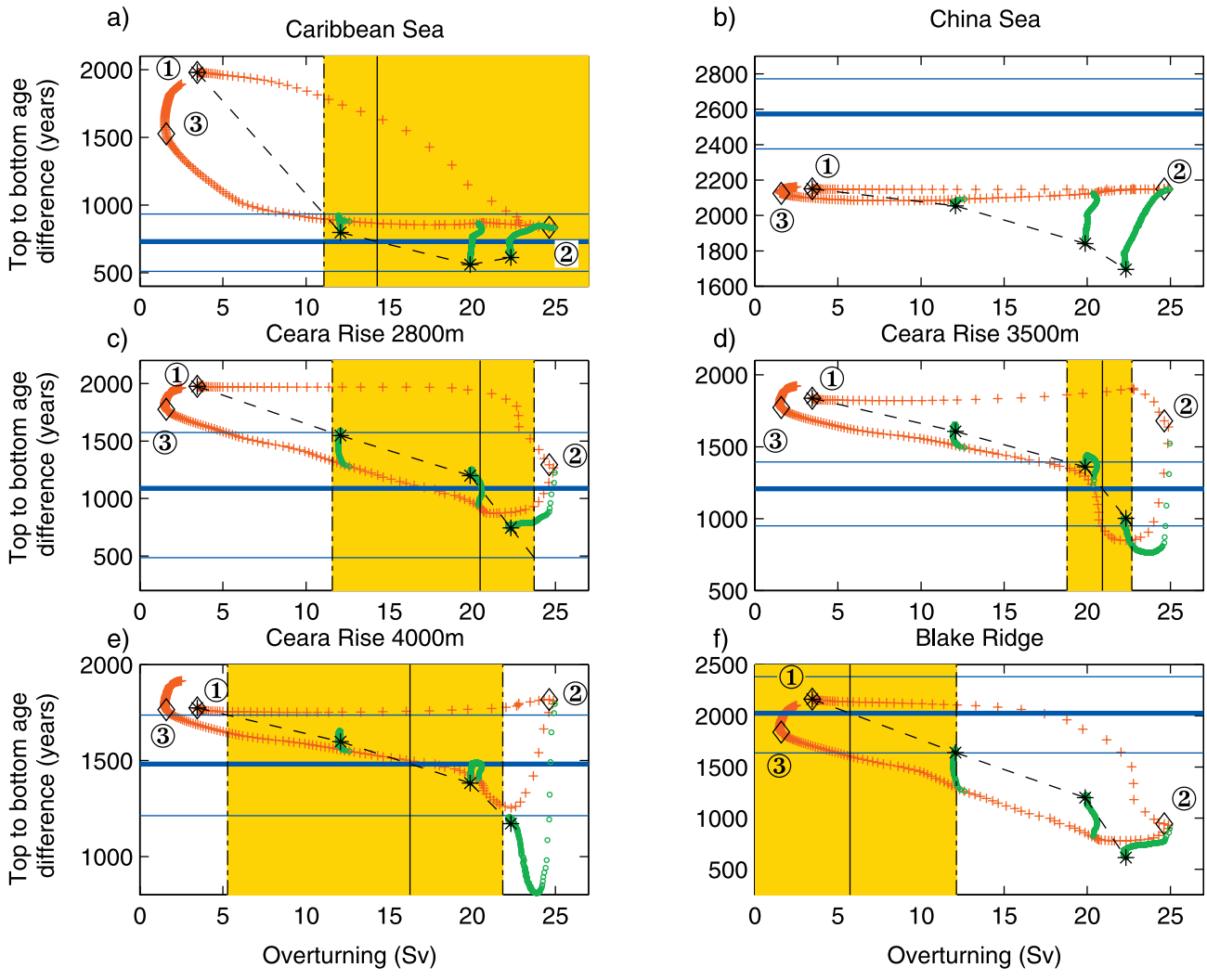

Figure 9. As Figure 7. Simulated atmospheric to bottom age difference (in years) are compared with redated data [*Adkins and Boyle*, 1997] (without reservoir age correction).

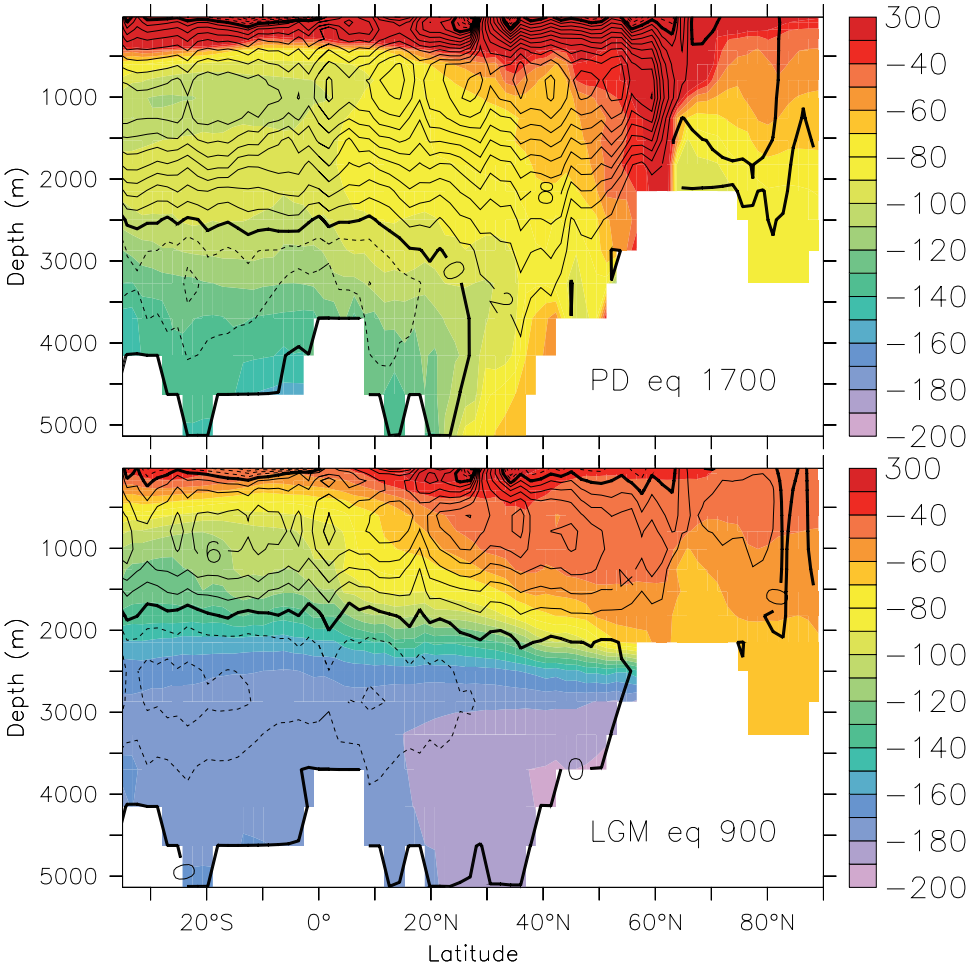

Figure 10. Distribution of the $^{14}C/^{12}C$ ratio (per mil), zonally averaged over the Atlantic. Isolines of the meridional stream function are represented as well. The upper panel shows annual means from the PD eq_1700 run, the lower panel annual means from the LGM eq_900 run.

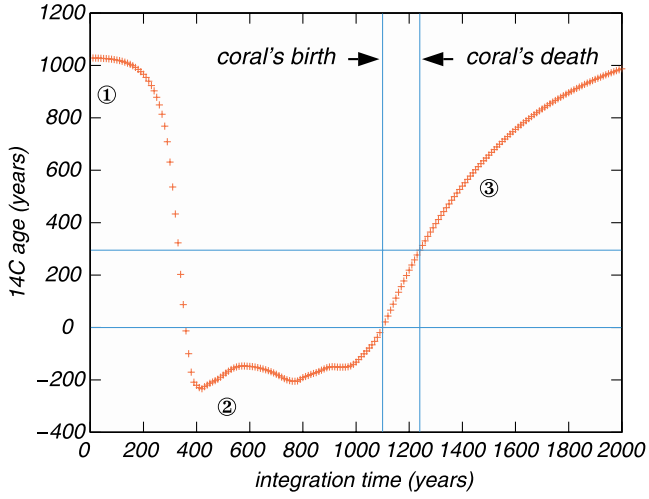

Figure 11. ^{14}C age (t) − ^{14}C age (t = 1100) at 38°N, 60°W and 1800 m depth during the LGM FWP experiment (red crosses). The results are shown every 10 integration years. The fictive deep sea coral grows between the points indicated by horizontal and vertical lines. Points 1, 2 and 3 indicate the end of the control run, and the minimum and maximum of freshwater forcing, respectively (see Figure 1).

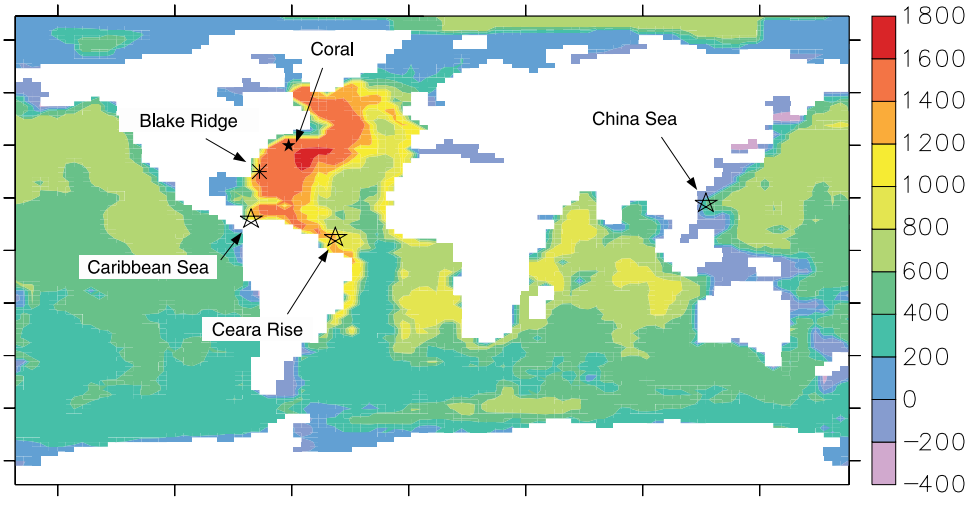

Figure 12. Difference between two extreme states (LGM control run (weak overturning) minus LGM eq_500 (strong overturning)) of the top to bottom age difference. The locations of the sea sediment cores and the deep sea coral are represented as well.